Review

Update on the Discovery of Efflux Pump Inhibitors against Critical Priority Gram-Negative Bacteria

Nina Compagne [1,†], Anais Vieira Da Cruz [1,†], Reinke T. Müller [2,†], Ruben C. Hartkoorn [3,*], Marion Flipo [1,*] and Klaas M. Pos [2,*]

[1] Univ. Lille, Inserm, Institut Pasteur de Lille, U1177—Drugs and Molecules for Living Systems, F-59000 Lille, France
[2] Institute of Biochemistry, Goethe-University Frankfurt, Max-von-Laue-Str. 9, D-60438 Frankfurt am Main, Germany
[3] Univ. Lille, CNRS, Inserm, CHU Lille, Institut Pasteur Lille, U1019—UMR 9017—CIIL—Center for Infection and Immunity of Lille, F-59000 Lille, France
* Correspondence: ruben.hartkoorn@inserm.fr (R.C.H.); marion.flipo@univ-lille.fr (M.F.); pos@em.uni-frankfurt.de (K.M.P.)
† These authors contributed equally to this work.

Abstract: Antimicrobial resistance (AMR) has become a major problem in public health leading to an estimated 4.95 million deaths in 2019. The selective pressure caused by the massive and repeated use of antibiotics has led to bacterial strains that are partially or even entirely resistant to known antibiotics. AMR is caused by several mechanisms, among which the (over)expression of multidrug efflux pumps plays a central role. Multidrug efflux pumps are transmembrane transporters, naturally expressed by Gram-negative bacteria, able to extrude and confer resistance to several classes of antibiotics. Targeting them would be an effective way to revive various options for treatment. Many efflux pump inhibitors (EPIs) have been described in the literature; however, none of them have entered clinical trials to date. This review presents eight families of EPIs active against *Escherichia coli* or *Pseudomonas aeruginosa*. Structure–activity relationships, chemical synthesis, *in vitro* and *in vivo* activities, and pharmacological properties are reported. Their binding sites and their mechanisms of action are also analyzed comparatively.

Keywords: efflux pump inhibitor; RND multidrug efflux pump; Gram-negative bacteria; antimicrobial resistance; antibiotic resistance breakers; AcrB; MexB

1. Introduction

The spread of antibiotic resistance represents a massive global health problem. While, on the one hand, multiresistant or even panresistant pathogens have become reality in clinics, the potential for discovering new compound classes has been recently revived but yet is often still in preclinical stages [1]. Over the past 30 years, the development of antimicrobial agents was almost exclusively limited to the modification of existing compounds [2,3]. Teixobactin, one of the last newly discovered classes of antibiotics, is effective against Gram-positive bacteria but not against Gram-negative pathogens such as *Acinetobacter baumannii*, *Pseudomonas aeruginosa*, and certain *Enterobacteriaceae*, whose resistance situation has been classified as particularly critical by the WHO [4,5]. For the Gram-negative bacterium *Pseudomonas aeruginosa*, inhaled murepavadin, a peptidomimetic antibiotic targeting the outer membrane protein LptD (involved in LPS-translocation), is currently in Phase I clinical trials. A recent report also describes Dynobactin, a peptide antibiotic targeting the BamA outer membrane protein insertion machinery, as an effective new antibiotic [6]. The latter two examples are the most recent promising antibacterial compounds and exemplify the need to focus scientific efforts on novel strategies, especially in the fight against Gram-negative bacteria.

In addition to possible acquired resistance mechanisms, Gram-negative bacteria already have a high intrinsic resistance to most clinical antibiotics, a property that can essentially be attributed to the combination of an additional outer membrane (OM) and the presence of powerful multidrug efflux pumps [7,8]. The highly asymmetric OM of Gram-negative bacteria, which is formed by lipopolysaccharides (LPS) on the outer leaflet and phospholipids on its inner leaflet, represents a significant permeability barrier, particularly for hydrophobic compounds such as bile salts, disinfectants, and most antimicrobials. Consequently, the OM reduces the uptake of antibiotics. However, as a passive barrier alone, it cannot influence the resulting intracellular equilibrium concentrations. Multidrug efflux transporters actively counteract influx across the outer (and inner) membrane. As a result, many antibiotics reach only sublethal concentrations at their sites of action within the bacterium [9]. Not surprisingly, multidrug efflux pumps have been found overexpressed in many clinical isolates [10,11]. As indicated by recent kinetic modeling studies and experiments, the interplay between slow uptake and active efflux appears to be finely tuned. Therefore, even small changes in one or both factors can dramatically increase intracellular drug concentrations, rendering the bacteria susceptible to antibiotic treatment [12,13]. This results in various possible approaches such as (i) the optimization of drugs for better influx and/or efflux avoidance [14–16], (ii) the permeabilization of the OM by additional chemosensitizers [2], or (iii) the inhibition of multidrug efflux pumps [17–19]. Synergistic approaches between (ii) membrane permeabilizers and (iii) efflux pump inhibitors (EPIs) can also be used to sensitize Gram-negative bacteria to antibiotics [20]. The inhibitory strategy appears to be the most versatile, since many antibiotics, including compounds that are ineffective per se for the reasons mentioned, can be (re-)used effectively against Gram-negative bacteria.

2. Tripartite RND Multidrug Efflux Pumps

Members of the tripartite Resistance Nodulation cell Division (RND) superfamily are the major multidrug efflux pumps in Gram-negative bacteria [21]. Tripartite RND efflux pumps consist of membrane fusion proteins (MFPs, also known as periplasmic adaptor proteins, PAPs), an RND core component, and an outer membrane factor (OMF), which together form an elongated complex that connects both the inner and outer bacterial membrane. The RND core component is present in the inner membrane (IM) as a homo- or heterotrimer. RND proteins recognize drug substrates and energize the drug efflux at the expense of the proton motive force (PMF). The MFPs build a hexameric ring on top of the RND proteins. In the active complex, this MFP forms a tubular structure, which connects to the open OMF porin in the outer membrane. As a result, substrates can be taken up by the RND core from the periplasm (or the outer leaflet of the IM) and removed from the cell by extrusion through the long MFP-OMF conduit across the OM [22–25] (see also [7] and [8] for reviews). Some pathogenic Gram-negative bacteria contain multiple clinically relevant tripartite RND efflux pumps with partially overlapping substrate specificities such as MexAB-OprM, MexCD-OprJ, MexEF-OprN, and MexXY-OprM from *Pseudomonas aeruginosa* or AdeABC, AdeFGH, and AdeIJK from *Acinetobacter baumannii* that are either constitutively expressed (MexAB and AdeIJK), induced by stress, or overexpressed due to mutation [26–28]. In other Gram-negatives such as *Escherichia coli* (AcrAB-TolC), *Salmonella enterica* (AcrAB-TolC), *Klebsiella pneumoniae* (AcrAB-TolC), *Campylobacter spp.* (CmeABC), and *Neisseria gonorrhoeae* (MtrCDE), single RND-tripartite systems appear to be dominant [28].

The value of RND efflux pumps as molecular targets is underscored by their propensity to support the acquisition of additional resistance mechanisms [29,30], their overexpression in dormant bacteria [31], and their role in cell-to-cell communication [32,33], biofilm formation [34], pathogenicity, and virulence [35]. Strategies against multidrug efflux pumps have been targeting their (a) expression [36], (b) complex assembly [37], or (c) the fully assembled active transporter.

This review focuses on synthetic RND efflux pump inhibitors that target the RND core component MexB or AcrB, or the MFP AcrA. A total of eight inhibitor classes with validated target-specific effects are described for their (i) structure–activity relationships, (ii) chemical synthesis, (iii) mode of action, (iv) *in vitro* activity, (v) pharmacological properties, and (vi) *in vivo* activity. The binding mode of AcrB substrates and inhibitors is also analyzed comparatively.

3. Efflux Pump Inhibitors

3.1. PAβN

PAβN (Phenylalanine-Arginine-β-Naphtylamide, **1**), also known as MC-207,110 (Figure 1), was discovered in 1999 by Microcide Pharmaceuticals and Daiichi Pharmaceutical Company as the first inhibitor of RND efflux pumps in Gram-negative bacteria. It was identified through the screening of approximately 200,000 synthetic and natural compounds in combination with a sub-inhibitory concentration of levofloxacin (an antibiotic substrate of RND efflux pumps), in order to find compounds that would potentiate the activity of this antibiotic on *Pseudomonas aeruginosa* [38–40]. This screening was performed using different engineered strains of *P. aeruginosa* that overexpressed either of the three main *P. aeruginosa* RND efflux pumps: MexAB-OprM (PAM1032), MexCD-OprJ (PAM1033), or MexEF-OprN (PAM1034) [41].

3.1.1. Structure–Activity Relationships (SARs)

PAβN (**1**) is a low-molecular-weight dipeptidic compound composed of an L-phenylalanine (AA$_1$) linked to an L-arginine (AA$_2$) substituted by a naphthylamine (Cap) (Figure 1).
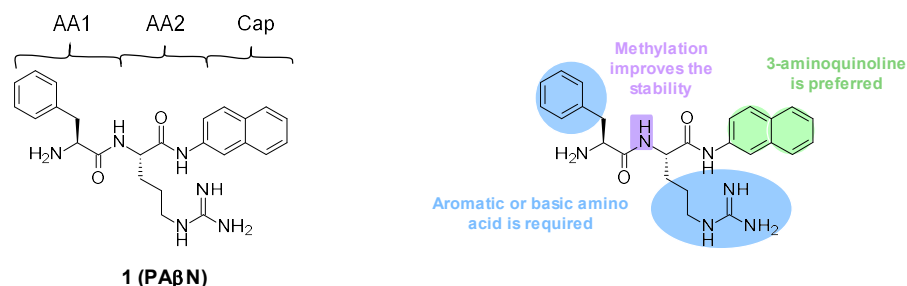

Figure 1. Structure of PAβN and summary of the different SARs.

Several structure–activity relationship (SAR) studies were performed in order to decrease the cytotoxicity and improve the potency and the ADME properties of PAβN (Figure 1) [39,42,43]. Amongst the more than 500 analogues that were synthesized and tested, the three main areas of modifications investigated were the nature of amino acids 1 and 2 and the cap moiety. Studies showed the following:

- **Replacement of AA$_1$ and AA$_2$:** It was described that amino acids 1 and 2 needed to contain both an aromatic and a basic moiety, though the order could be inverted [39,42]. Replacement of L-phenylalanine with an L-homo-phenylalanine led to a 2-fold improvement in EPI potency. In addition, ornithine or an aminomethylproline was accepted as an alternative basic amino side chain [39,43].
- **Substitution of the amide bond:** Methylation of the amide between AA$_1$ and AA$_2$ led to a slight improvement in compound potency and plasma stability [39].
- **Modification of the cap side:** Replacement of the naphthyl moiety by other fused rings such as 5-aminoindan and 6-aminoquinoline was tolerated [39]. However, the introduction of a 3-aminoquinoline moiety was preferred to reduce the cytotoxicity on mammalian cells *in vitro* [39].

These structure–activity relationship studies have allowed the identification of several compounds, such as **2**, **3**, **4** (MC-02,595), and **5** (MC-04,124) (Figure 2).
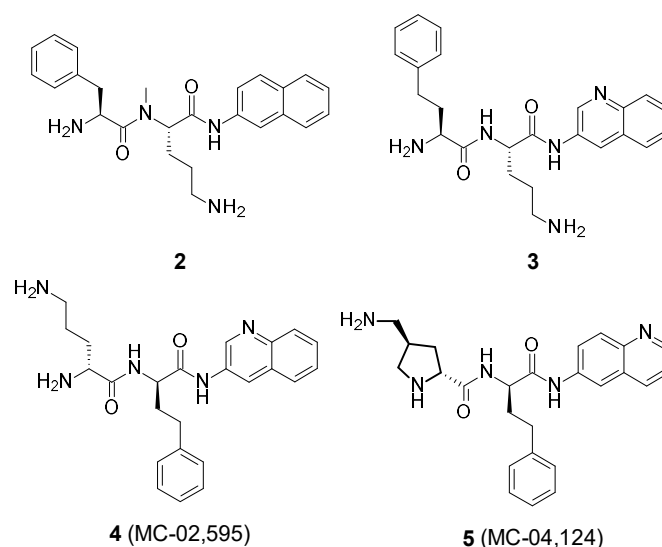
Figure 2. Structure of PAβN analogues.

3.1.2. Chemical Synthesis

PAβN and its analogues were synthesized by standard peptide solid phase synthesis (Scheme 1) [44]. Starting from the carbonate resin **6**, which was synthesized in two steps, the first amino acid was grafted as a lithium salt. The lithium salt was then converted to tetrabutylammonium salt by reaction with tetrabutylammonium fluoride (TBAF). Intermediate **8** was then activated using 2,4-dinitro-1-fluorobenzene (**9**) and reacted with the second amino acid to form intermediate **11**. The Cap moiety was finally introduced after activation of the carboxylate with EDCI (1-ethyl-3-(3-dimethylaminopropyl)carbodiimide) and HOBt (hydroxybenzotriazole), and then the resin was removed under acidic conditions using trifluoroacetic acid (TFA) to release the final desired compound **13**.
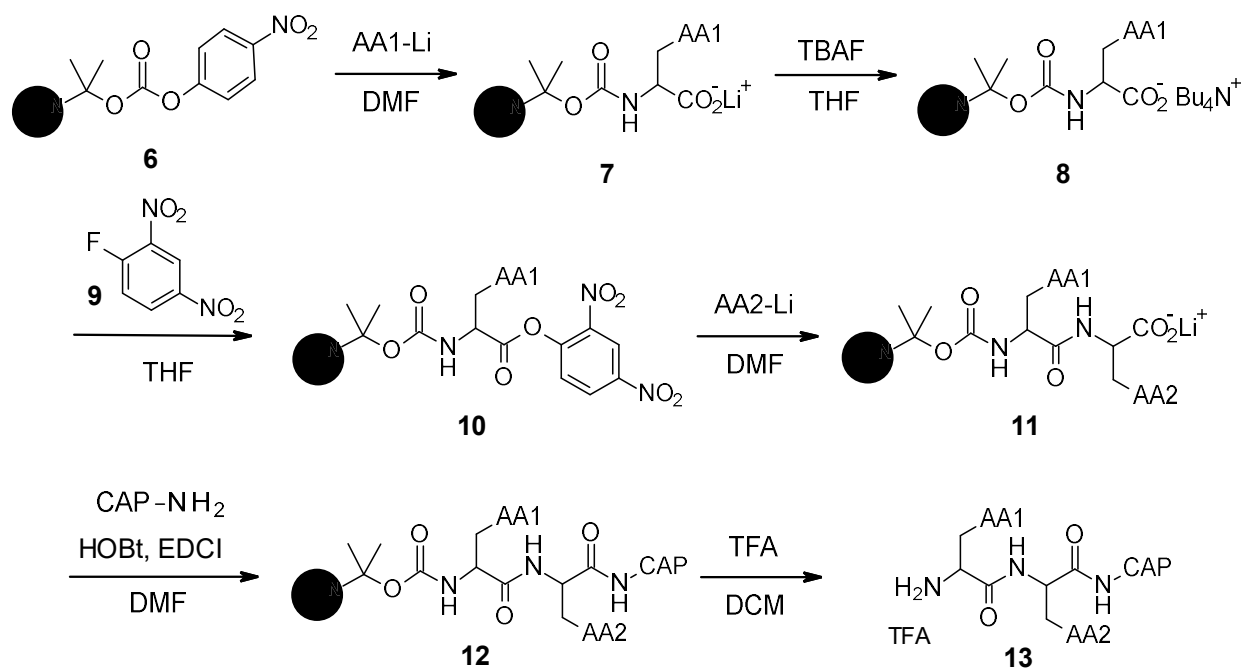
Scheme 1. Chemical synthesis of PAβN and its analogues.

3.1.3. *In Vitro* Activity

PAβN inhibits the three RND pumps of *P. aeruginosa* (MexAB-OprM, MexCD-OprJ, and MexEF-OprN) and is also a substrate of these pumps, indicating it acts as a competitive inhibitor. It has broad-spectrum efflux pump inhibitory activity and is, therefore, able to potentiate the activity of different families of antibiotics such as fluoroquinolones, macrolides, oxazolidinones, chloramphenicol, and rifampin but not aminoglycosides [40,41].

PAβN was reported to have no intrinsic bacterial activity but PAβN can permeabilize the membrane of PAM2035 *P. aeruginosa* strains (deficient for MexAB-OprM efflux pump) due to its cationicity [45]. Indeed, being protonated at physiological pH, PAβN can displace divalent cations that bridge phosphate groups of OM LPS, leading to OM instability. In *P. aeruginosa* WT strains or strains overexpressing the three Mex RND efflux pumps, the minimum inhibitory concentration (MIC) of PAβN was 512 μg/mL [39,41]. At a concentration of 20 μg/mL, PAβN is able to boost the activity of levofloxacin on *P. aeruginosa* by 16-fold, and up to 64-fold on strains overexpressing the Mex RND efflux pumps (where basal susceptibility was lower). Analogues identified in the SAR studies (**2** and **3**, minimal potentiating concentration (MPC_8) of 5 μg/mL [39]; **4** and **5**, MPC_8 = 10 μg/mL [43]) showed similar efflux pump inhibition to that of PAβN (MPC_8 = 10 μg/mL).

At a concentration of 25–50 μ g/mL, PAβN was found to also reduce the MICs of several β-lactam antibiotics (piperacillin, cefotaxime, ceftazidime, and ciprofloxacin) against *P. aeruginosa* WT by a factor of 2 to 4 (and by a factor up to 42 on *dacB* strains that overexpress AmpC) [45].

PAβN and its analogues were also shown to inhibit RND efflux in *Escherichia coli* [41,46], as well as the AdeFGH RND efflux pump of *Acinetobacter baumannii*, where it was described to boost the activity of clindamycin, chloramphenicol, and trimethoprim on different clinical isolates of *A. baumannii* (AB005, AB010, and AB014) [47].

3.1.4. Pharmacological Properties

PAβN is unstable in murine serum, likely due to the cleavage of the peptide bond between AA_1 and AA_2 [42]. Analogue **4** (**MC-02,595**), where AA_1 and AA_2 are changed, had greatly improved stability in murine serum (95% recovery after 2 h). Similarly, compound **2,** where the nitrogen of the amide bond is methylated, was found to better resist cleavage by serum proteases.

PAβN and several analogues such as compound **4** were reported to be toxic for mice after intravenous administration (LD_{50} < 25 mg/kg, MLD (minimal dose causing lethality to ≥66% of the animals tested) <25 mg/kg) [43]. As mentioned previously, a basic side chain (such as ornithine) for AA_1 or AA_2 was found to be critical for effective efflux pump inhibition; however, this moiety was also identified as the major contributor to compound toxicity. Replacement of the ornithine moiety by an aminomethylproline (**5**, **MC-04,124**) allowed a 4-fold decrease in toxicity (MLD > 100 mg/kg) in rodents, while maintaining the same level of inhibition.

Pharmacokinetic profiling in rats [48] showed that in contrast to serum concentrations, a single dose of compound **5** led to high concentrations in several organs (kidneys, liver, and lungs) after 24 h. Similarly, repeated doses provoked a significant accumulation in these organs, and the accumulation in the kidneys led to nephrotoxicity [35].

3.1.5. *In Vivo* Activity

Compound **2** was evaluated in a neutropenic mouse model of thigh infection with *P. aeruginosa* overexpressing MexAB-OprM (PAM1032) in combination with levofloxacin [39]. Immunosuppressed male CFW mice were infected by 10^5 CFU of *P. aeruginosa* PAM 1032 intramuscularly and treated with levofloxacin subcutaneously at 30 mg/kg and compound **2** intraperitoneally at 30 mg/kg. At these doses, levofloxacin alone and compound **2** alone each resulted in bacterial growth similar to untreated mice. The combination compound **2**/levofloxacin led to a 3-log reduction in CFU after 4 h. Compound **5** (**MC-04,124**)

was also evaluated in an *in vivo* model of infection in combination with levofloxacin and shown to be similarly effective [43].

During the development of this chemical series, it was shown that the basic moieties of PAβN and its analogues were essential for activity. However, these moieties are associated with unfavorable pharmacokinetic and toxicological profiles, explaining why the development of this chemical series was suspended [40]. As a consequence, these compounds are only used as research tools due to their broad-spectrum EPI activity to understand the role of efflux pumps in antibiotic resistance in *P. aeruginosa* and other Gram-negative bacteria.

3.2. NMP and Arylpiperazines

Arylpiperazines were first described by Bohnert and Kern in 2005 as being able to reverse multidrug resistance in *E. coli* (Figure 3). [49]. These compounds were identified through high-throughput screening of synthetic and commercially available *N*-heterocyclic compounds, on two *E. coli* strains overexpressing *acrAB* (3-AG100MKX) and *acrEF* (2-DC14PS), in the presence of levofloxacin (sub-inhibitory concentrations).

3.2.1. Structure-Activity Relationships

Following the identification of the arylpiperazine series from the screening, different structure–activity relationship studies were performed [49]. It has been highlighted that the efflux pump inhibitory activity of these compounds depends on four parameters (Figure 3):

- **The size of the linker** between the aromatic ring and the piperazine: Linker elongation led to an improvement in potency.
- **The substitution of the phenyl ring:** Substitution of the benzene ring with a halogen-containing moiety increased compound potency. In particular, the introduction of a trifluoromethyl group in the *meta* position was preferred (8-fold improvement in boosting activity).
- **The nature of the aromatic ring:** Replacement of the phenyl ring by a naphthyl ring led to a 5-fold improvement in potency.
- **The substitution of the piperazine**: Substitutions of the piperazine ring were not tolerated and led to decreased potency.

The SAR studies have allowed the discovery of NMP (**14**, 1-(1-naphtylmethyl)-piperazine) as one of the most potent arylpiperazines (levofloxacin-MRC$_4$ = 50 µg/mL) (Figure 3) [49].
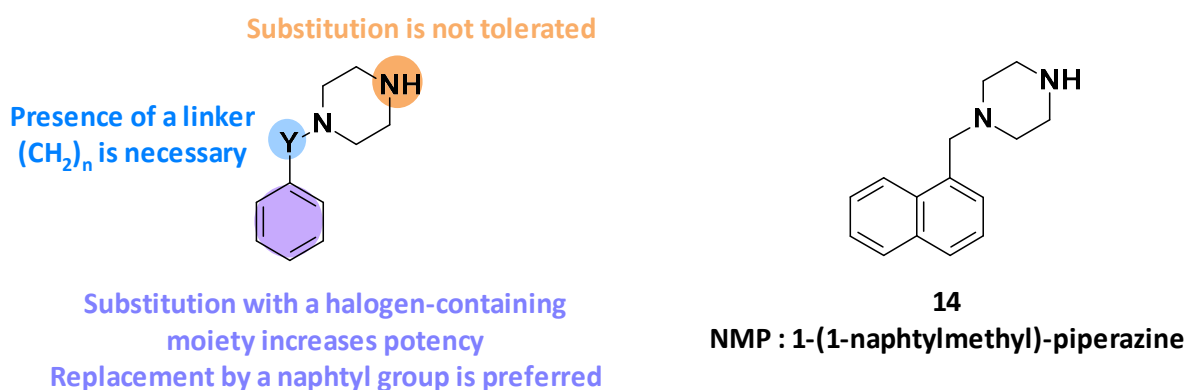

Figure 3. Summary of the different SARs leading to the discovery of NMP (**14**).

3.2.2. Chemical Synthesis

NMP synthesis was described in three steps from 1-(chloromethyl)naphthalene **15** (Scheme 2) [50]. The first step involved a Finkelstein reaction to generate the iodide derivative **16**, followed by a nucleophilic substitution with Boc-piperazine and cleavage of the Boc group in acidic media.
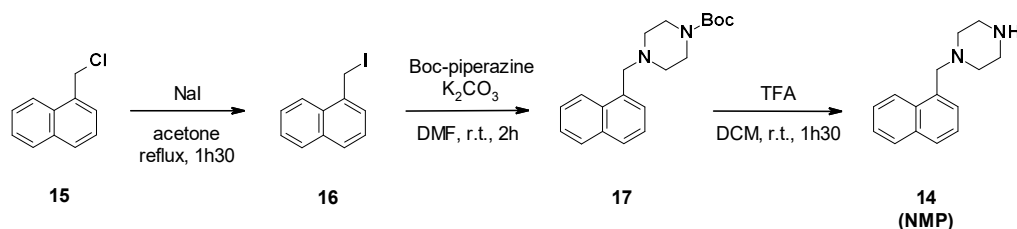
Scheme 2. Chemical synthesis of NMP (**14**).

3.2.3. *In Vitro* Activity

NMP by itself has no intrinsic antibacterial activity (MIC = 400 μg/mL) on *E. coli* strains overexpressing or deficient in RND efflux pumps [49].

At a concentration of 100 μg/mL, NMP is able to increase the intracellular accumulation of levofloxacin in *E. coli* strains overexpressing *acrAB* (3-AG100MKX) [49]. It has also been shown that NMP at 100 μg/mL reduces the MIC of levofloxacin by 16-fold on *E. coli* (2-DC14PS) overexpressing *acrEF* and by 8-fold on *E. coli* 3-AG100MKX.

NMP was also reported to boost the activity of several antibiotics such as oxacillin, rifampicin, chloramphenicol, various fluoroquinolones (levofloxacin, ciprofloxacin, norfloxacin, enoxacin, and pefloxacin), different macrolides (clarithromycin, erythromycin, and azithromycin), clindamycin, doxycycline, linezolid, and nitrofurantoin on *E. coli* overexpressing AcrAB-TolC [49]. For example, at 100 μg/mL, it reduced the MIC of oxacillin, rifampicin, chloramphenicol, and clarithromycin by 4- to 8-fold and the MIC of linezolid by 8- to 32-fold on *E. coli* strains (3-AG100MKX and 2-DC14PS) overexpressing efflux pumps. As expected, the addition of NMP has no effect on efflux-pump-deficient strains (such as 1-DC14PS), demonstrating that the boosting effect of NMP is due to the inhibition of the efflux pump. Furthermore, it has no effect on ketolides (telithromycin), glycopeptides, aminoglycosides, trimethoprim/sulfamethoxazole, and fosfomycin [49].

NMP was also tested on clinical isolates and showed moderate boosting activity on multi-drug resistant (MDR) Enterobacterales (*E. coli*, *E. aerogenes*, *K. pneumoniae*) [51,52] and restored partial susceptibility to fluoroquinolones particularly on *E. coli*. At a concentration of 100 μg/mL, it reduced the MIC of levofloxacin by 4-fold on more than 50% of fluoroquinolone-sensitive *E. coli* strains and more than 70% of the fluoroquinolone-resistant strains.

Noteworthily, NMP was able to partially reverse drug resistance in *A. baumannii* [53]. At 100 μg/mL, it reduced the MIC of several antibiotics (e.g., levofloxacin, ciprofloxacin, chloramphenicol, and linezolid) by 4-fold or more on the *A. baumannii* ATCC 1906 strain and on SB13 and U10247 clinical strains.

3.2.4. Pharmacological Properties

The arylpiperazine backbone of NMP may be associated with a serotonergic agonist effect, rendering it potentially toxic for clinical use [54]. No *in vivo* experiment has been reported for the arylpiperazine series.

3.3. D13-9001

D13-9001 (**19**) was designed as a specific inhibitor of MexAB-OprM of *P. aeruginosa* and is characterized by a pyridopyrimidine core (Figure 4). This compound was obtained after optimization of an initial hit compound (**18**) identified by high-throughput screening.

D13-9001 binds to MexB and AcrB in the deep binding pocket region known as the hydrophobic trap and inhibits the efflux of drugs by MexAB-OprM and AcrAB-TolC, respectively [55].

3.3.1. Structure–Activity Relationships

Evaluation of the hit compound **18** revealed that it was highly bound to plasma proteins, limiting its potency in the presence of serum [56]. This can be explained by the

presence of a carboxylic acid function and the relative hydrophobicity of the compound. To solve this issue, the authors introduced polar moieties at position C4 of the thiazole ring or replaced the phenyl ring linked to the carboxylic acid. However, these modifications led to inactive compounds. The substitution of the styrene with a pyridine linked to an ether or ethylene group decreased the plasma protein binding (PPB), but also reduced the potency of the compounds [56].
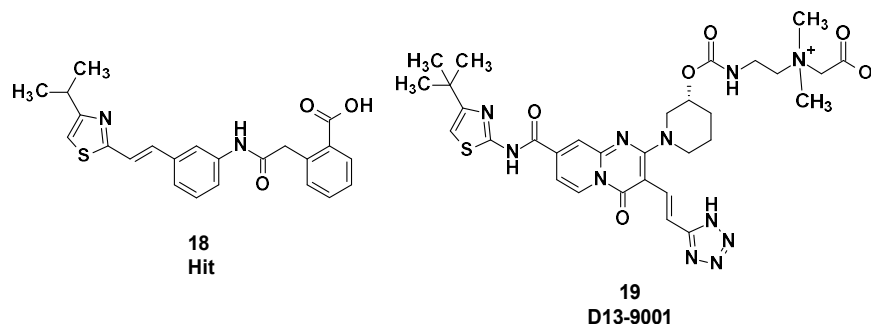

Figure 4. Structure of the hit compound **18** and of D13-9001 (**19**).

Subsequently, Nakayama et al. considered a change in scaffold by introducing a quinolone, leading to ineffective compounds, or alternatively introducing a pyridopyrimidine, which resulted in a decrease in potency but greatly reduced PPB. In parallel, it was shown that the substitution of the carboxylic acid with a bioisostere such as a tetrazole improved the potency [57].

Next, the introduction of a substituent in position C2 of the pyridopyrimidine core was considered. Cyclic amines led to the most potent compounds, and substitution of those cyclic amines with alcohols or carbamates was tolerated. The tetrazole was spaced from the pyridopyrimidine core with olefins, leading to an increase in potency. However, only the *E* isomer displayed activity, and a photochemical isomerization was observed with ambient light [58]. To prevent this phenomenon, the electron-donating ethylene in position C7 was replaced by an electron-withdrawing amide. As a result, the *E*-isomer was stable after exposure to ambient light (*E*/*Z* ratio after 240 min: 99/1). Regarding the cyclic amine in position C2, a carbamate in the (*R*) configuration was revealed to be more potent than the corresponding (*S*) enantiomer [59].

Carbon-substituted analogues with aryl or alkyl moieties in position C2 were also evaluated, but this led to an increase in lipophilicity, resulting in a lower solubility and greater PPB [60,61].

To improve solubility, highly water-soluble moieties, such as quaternary ammonium salt, were added. This led to the identification of D13-9001 (**19**), a specific inhibitor of MexAB-OprM in *P. aeruginosa* [62] (Figure 5).

3.3.2. Chemical Synthesis

D13-9001 was obtained in a 10-step synthesis starting with 2-acetamidopyridine-4-carboxylic acid (Scheme 3). First, a coupling reaction was performed between 4-*tert*-butylthiazol-2-amine and the synthesized acyl chloride **21**. The aniline was then deprotected by the reaction with ethanol in acidic conditions. This allowed for the formation of the pyridopyrimidine core through the reaction of **23** with bis(2,4,6-trichlorophenyl)malonate (TCPM). Subsequent formylation by the Vilsmeier–Haack reagent formed using phosgene in DMF yielded the corresponding aldehyde intermediate **25**. The olefin derivative **26** was then synthesized by condensation with 2-(1*H*-tetrazol-5-yl)acetic acid protected by a PMB (*p*-methoxybenzyl) group, followed by decarboxylation. An aromatic nucleophilic substitution with (3R)-piperidin-3-ol hydrochloride was then performed after activation of the phenol with diphenyl phosphoryle chloride to yield intermediate **27**. Subsequent reaction with carbonyldiimidazole (CDI) and *N'*,*N'*-dimethylethane-1,2-diamine gave the

corresponding carbamate **28**. The tertiary amine was then alkylated using *tert*-butyl-2-bromoacetate, leading to ammonium **29**. Finally, the tetrazole was deprotected by reaction with trifluoroacetic acid in anisole to yield D13-9001 (**19**) [62].
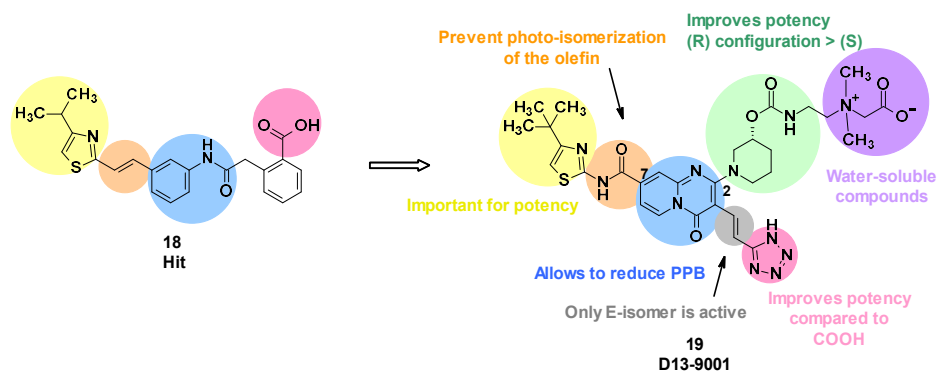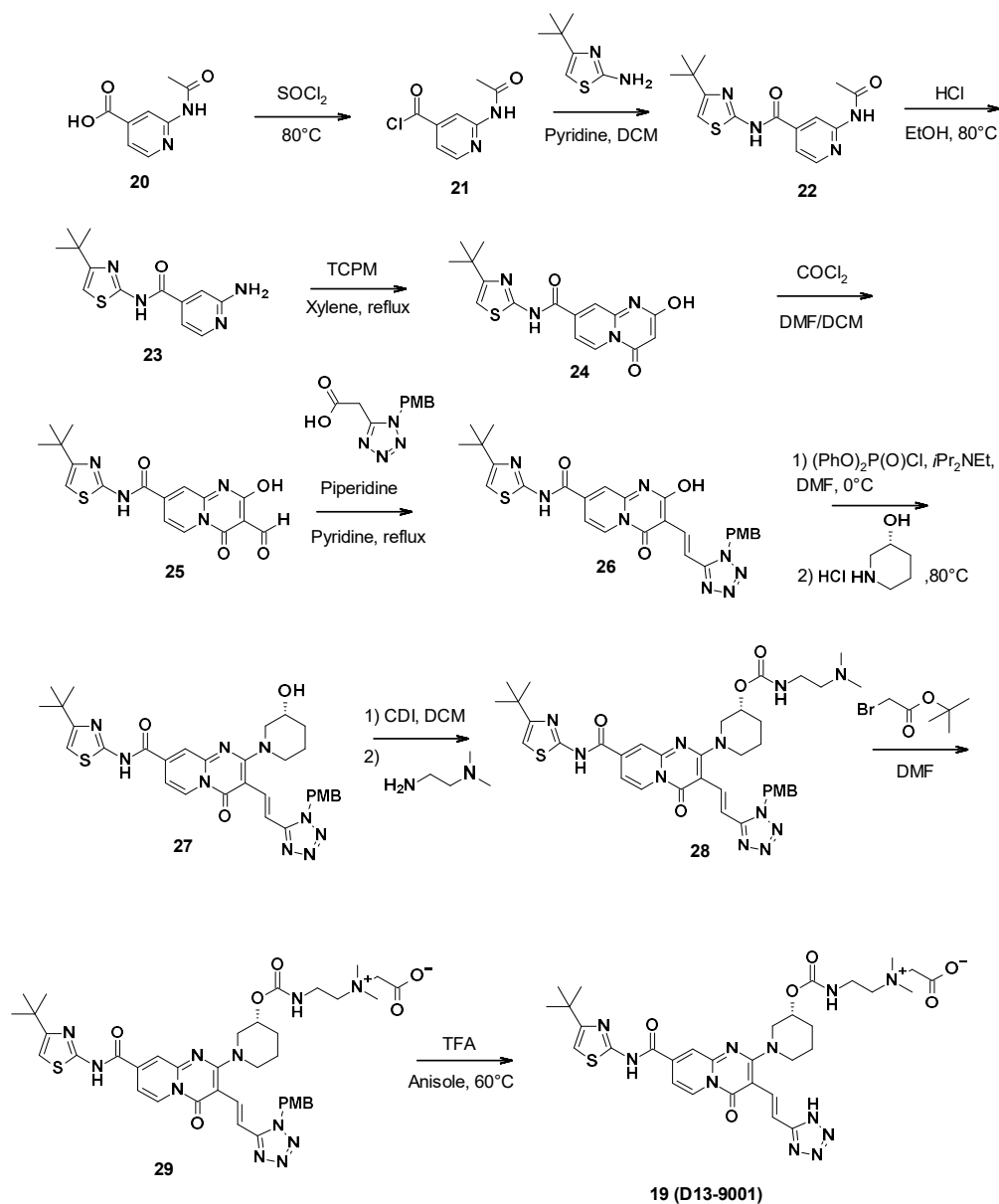

Figure 5. Summary of the structure–activity leading to D13-9001.

Scheme 3. Description of the synthesis pathway leading to D13-9001.

3.3.3. *In Vitro* Activity

The SAR studies identified D13-9001 as a lead compound, characterized by a lower potency but improved physicochemical properties compared to the hit **18**, such as better solubility and reduced plasma protein binding. *In vitro*, a concentration of 2 μg/mL of D13-9001 decreased the MIC of levofloxacin and aztreonam 8-fold in a *P. aeruginosa* Δ*mexCD*Δ*oprJ*_Δ*mexEF*Δ*oprN* strain overexpressing MexAB-OprM [62]. The K_D values of D13-9001 binding to purified AcrB and MexB were 1.15 and 3.57 μM, respectively [50].

3.3.4. Pharmacological Properties

In addition to its demonstrated *in vivo* efficacy, D13-9001 is very soluble (747 μg/mL at pH 6.8) due to the presence of the quaternary ammonium. It also shows a linear PK profile in rats and monkeys after IV administration. A plasmatic concentration of 7.64 μg/mL was measured after the intravenous administration of a 5 mg/kg dose. The half-life was comprised of between 0.18 h in rats and 0.41 h in monkeys. Moreover, D13-9001 exhibited a good safety profile in an acute toxicity assay [62]. Structural studies showing binding of D13-9001 to the hydrophobic trap of MexB and AcrB (discussed under Section 4.3) were followed up by multiple molecular dynamics studies [63].

3.3.5. *in vivo* Activity

The combination D13-9001/aztreonam was evaluated *in vivo* in an acute *P. aeruginosa* pulmonary infection rat model. The lowest dose of D13-9001 tested (1.25 mg/kg) in combination with 1000 mg/kg of aztreonam resulted in more than 62% survival after 7 days, whereas aztreonam alone led to only 12.5% survival, showing the efficacy of the designed EPI [62].

Since the publication of Yoshida et al. in 2007, no recent advances have been reported regarding the preclinical or clinical development of D13-9001.

3.4. MBX Compounds

Pyranopyridines were first described in 2014 by the US company MicroBiotix as AcrAB-TolC efflux pump inhibitors in *E. coli* [64]. Cell-based high-throughput screening of 183,400 small molecules led to the identification of MBX2319 (**30**) as a potentiator of ciprofloxacin in *E. coli*.

3.4.1. Structure—Activity Relationships

MBX2319 (**30**) is composed of a pyridine core substituted by five groups (Figure 6). In order to improve the potency, solubility, and metabolic stability of this compound, structure–activity relationship studies have been performed, in which the different substituents have been modified (Figure 6) [65].

- **Replacement of the nitrile group**: Only two examples were synthesized due to synthetic problems, one with an *N*-hydroxyamide and the other with an amide, but these modifications led to a decrease in potency (MPC_4 (levofloxacin and piperacillin) > 100 μM).
- **The oxidation of the sulfide group** to sulfoxide or sulfone also led to a decrease in potency.
- **Modification of alkyl linker**: The deletion of the chain on the sulfide, the modification of the chain size (one or three carbons), and the oxidation of the chain led to a total loss of activity.
- **Modification of gem-dimethyl moiety**: Replacement of gem-dimethyl substituent by hydrogen atoms also led to a total loss of activity.
- **Modification of the morpholine ring**: The morpholine was replaced by a variety of acyclic or cyclic (5,6,7-membered rings) amine. In general, the replacement was tolerated, but the introduction of substituents with basic amines was found to be associated with moderate/strong cytotoxicity. Only the introduction of a 2,6-dimethyl group allowed a good balance between activity and cytotoxicity.

- **Substitution/modification of the phenyl ring**: The introduction of substituents on the phenyl ring was tolerated, and the activity of the compounds depended on the substituent in the *para* position. The introduction of a neutral or basic substituent on the phenyl ring seemed to improve the activity.

The SARs allowed the discovery of three compounds: MBX3132 (**31**), MBX3135 (**32**), and MBX4191 (**33**) (Figure 6) [65].
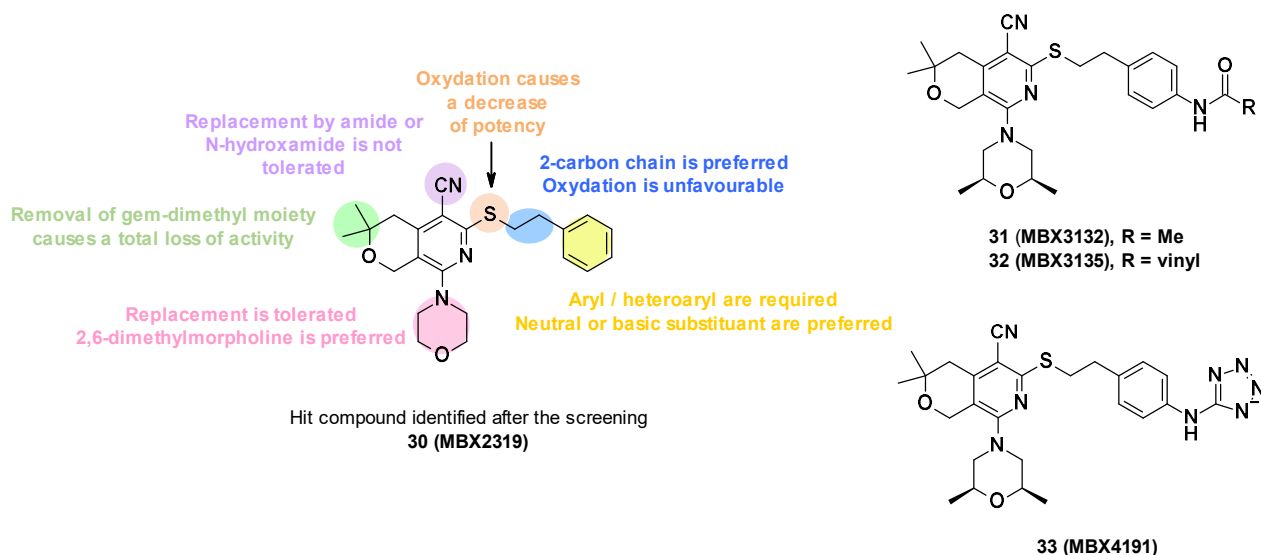

Figure 6. Structure of the hit MBX2319 (**30**), summary of the SARs performed, and structures of the three lead compounds.

3.4.2. Chemical Synthesis

The different pyranopyridines were synthesized via a three-step synthetic approach (Scheme 4) [65]. It started with a three-component coupling between pyranone, malonitrile, and disulfite carbon to form the thione **35**. The reaction of this thione with cyclic amines led to the formation of different substituted dihydropyranopyridines **36,** which were then alkylated to produce the corresponding desired product **37**.
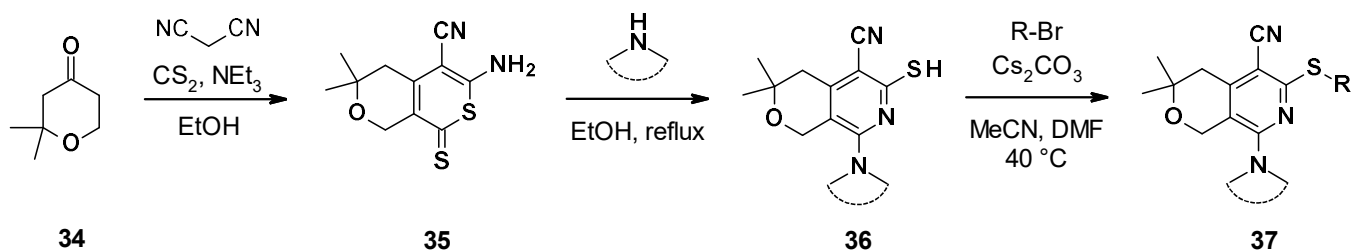
Scheme 4. Chemical synthesis of the MBX compounds.

3.4.3. *In Vitro* Activity

Pyranopyridine compounds did not exhibit membrane-disruptive properties and did not possess intrinsic antibacterial activity (MIC > 100 μg/mL) [64].

MBX2319 (**30**) potentiated the activity of several families of AcrB substrate antibiotics: Fluoroquinolones (ciprofloxacin, levofloxacin), β-lactams (piperacillin, oxacillin), and chloramphenicol [64]. Indeed, at 3.13 μM, it decreased the MIC of ciprofloxacin, levofloxacin, and piperacillin by a 2-, 4-, and 4-fold, respectively, on *E. coli* WT strain (AB1157) and by 4- to 8- fold on *E. coli* strains overexpressing efflux pumps (285 and 287). It does not boost antibiotics in efflux-deficient strains.

Moreover, MBX2319 improved the antibacterial activity of levofloxacin and ciprofloxacin by 2- to 5- fold on several other Gram-negative bacteria: *Shigella flexneri*, *Enterobacter aerogenes*, *Salmonella enterica*, and *Klebsiella pneumoniae,* and presented a weak activity with *P. aeruginosa* strains [64].

MBX3132 (**31**, MPC_4 of levofloxacin and piperacillin: 0.1 μM) and MBX3135 (**32**, MPC_4 of levofloxacin and piperacillin: 0.1 and 0.05 μM) are 30-fold more potent against *E. coli* than MBX2319 (**30**, MPC_4 levofloxacin and piperacillin: 3.1 μM) [65].

3.4.4. Mode of Action

Co-crystal structures of pyranopyridines were obtained and showed that MBX2319 binds to the periplasmic domain of AcrB (AcrBper) in the hydrophobic trap in the AcrB T protomer [66]. A detailed description of the interaction of the inhibitor with AcrB is given below (Section 4.3).

3.4.5. Pharmacological Properties

While the hit MBX2319 showed a very low solubility (12 μM) and very high instability in mouse liver microsome (MLM) and human liver microsome (HLM) (0% remaining after 1 h at 37 °C in the presence of NADPH), the SARs performed allowed researchers to identify compounds with better physico-chemical and pharmacokinetic properties [65]. Compounds with ionizable groups had better solubility (MBX4191: >100 μM [67]) than neutral analogues (50 μM for MBX3132, 25 μM for MBX3135). Moreover, the introduction of a dimethylmorpholinyl group led to more stable compounds in microsomes (49% in MLM and 100% in HLM remaining after 1 h for MBX3135, 97% in MLM remaining after 1 h for MBX4191 [65,67]).

MBX compounds showed moderate cytotoxicity on mammalian cells (HeLa) (CC_{50} > 100 μM for MBX2319, CC_{50} = 60.5 μM for MBX3132, CC_{50} = 62.4 μM for MBX3135, and CC_{50} = 47 μM for MBX4191) [65,67].

3.4.6. *In Vivo* Activity

MBX4191 (**33**) showed good serum exposure after intraperitoneal and intravenous doses of 10 and 100 mg/kg in mice [68]. The compound exhibited favorable pharmacokinetic properties allowing its evaluation in a mouse model of sepsis. MBX4191 potentiated the activity of levofloxacin in mice infected with a drug-susceptible strain of *E. coli* and potentiated minocycline in mice infected with a minocycline-resistant strain of *K. pneumoniae* [67].

3.5. 2H-Benzo[h]chromene Series

WK2 (**42**) is an AcrB inhibitor characterized by a 2*H*-benzo[h]chromene core developed by Wang et al. [69]. This compound is the result of several medicinal chemistry programs. The authors first selected the 2-naphtamide core following an in silico screening. This led to the identification of 4-isopentyloxy-2-naphthamide as a moderate AcrB inhibitor (compound **A3**, **38**) [70,71]. The naphthamide moiety was then replaced by a methoxy-2,3-naphthalimide ring, yielding compound **A5** (**39**) [72]. Finally, the combination of the naphthamide approach with WD6 (**41**) [73], itself originating from the optimization of NDGA (**40**, nordihydroguaiaretic acid) [74], led to the 2*H*-benzo[h]chromene derivatives (Figure 7).

3.5.1. Structure–Activity Relationships

Firstly, the structure of the core was investigated (Figure 8). It was revealed that chromanone derivatives were less potent overall than the corresponding 2*H*-benzo[h]chromene derivatives. Then, two points of derivatization were defined around the 2*H*-benzo[h]chromene core: The R substituent in position C5 and the R′ substituent on the phenyl ring linked in position C7. Concerning position C5, small polar groups were more favorable for the potency of the compounds. This could be explained by a possible hydrogen bond network

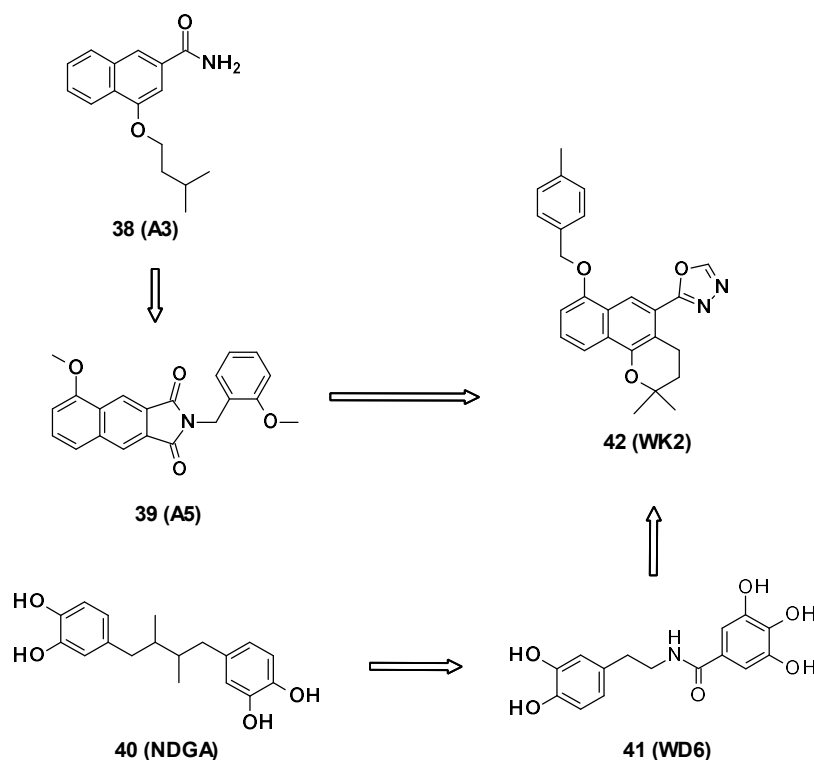between the compound, a water molecule, and residue Gln176 of AcrB, as described in the docking study.

Figure 7. Structures of compounds A3 (**38**), A5 (**39**), NDGA (**40**, nordihydroguaiaretic acid), WD6 (**41**), and WK2 (**42**).
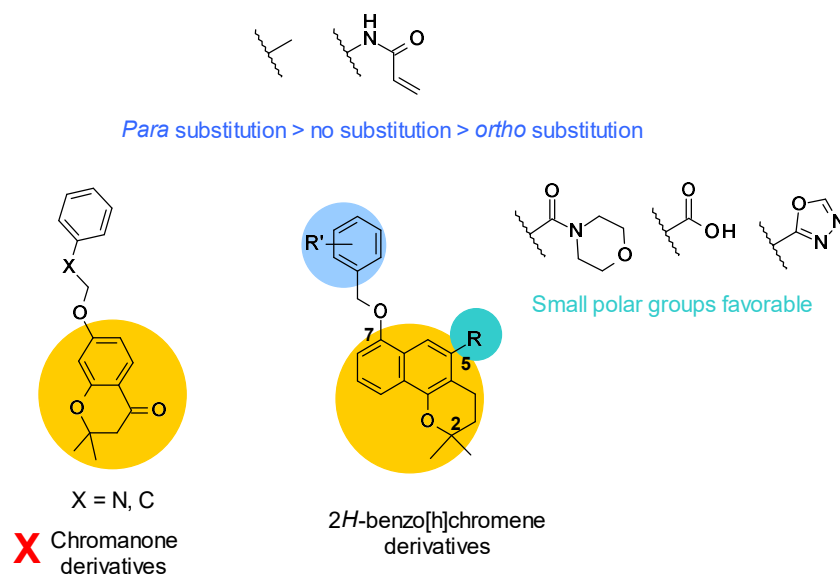

Figure 8. SARs summary for 2*H*-benzo[h]chromene derivatives.

Lastly, a methyl group or acrylamide as R′ substituent gave the most potent compounds. To note, *para* substitution was more favorable compared to no substitution or *ortho* substitution [69] (Figure 8).

3.5.2. Chemical Synthesis

WK2 (**42**) was obtained in nine steps (Scheme 5). First, the phenol function of sal-icylaldehyde was protected with benzyl chloride. A Stobbe condensation with diethyl succinate allowed the synthesis of the corresponding α,β-unsaturated ester **45**. The forma-tion of the second aromatic ring was performed in acetic anhydride under reflux conditions. Then, the acetyl group was removed with potassium carbonate in methanol, allowing the [3+3] cycloaddition with 3-methyl-2-butenal to form the benzo[h]chromene core of compound **48**. The oxadiazole ring was obtained after the reaction with hydrazine hydrate to form the hydrazide **49**, followed by triethyl orthoformate to close the ring. Catalytic hydrogenation allowed the deprotection of the phenol function and reduced the double bond to form the 2*H*-benzo[h]chromene core of compound **51**. Finally, this intermediate reacted with 4-methyl-benzyl halide and potassium carbonate to yield compound **WK2** (**42**) [69].
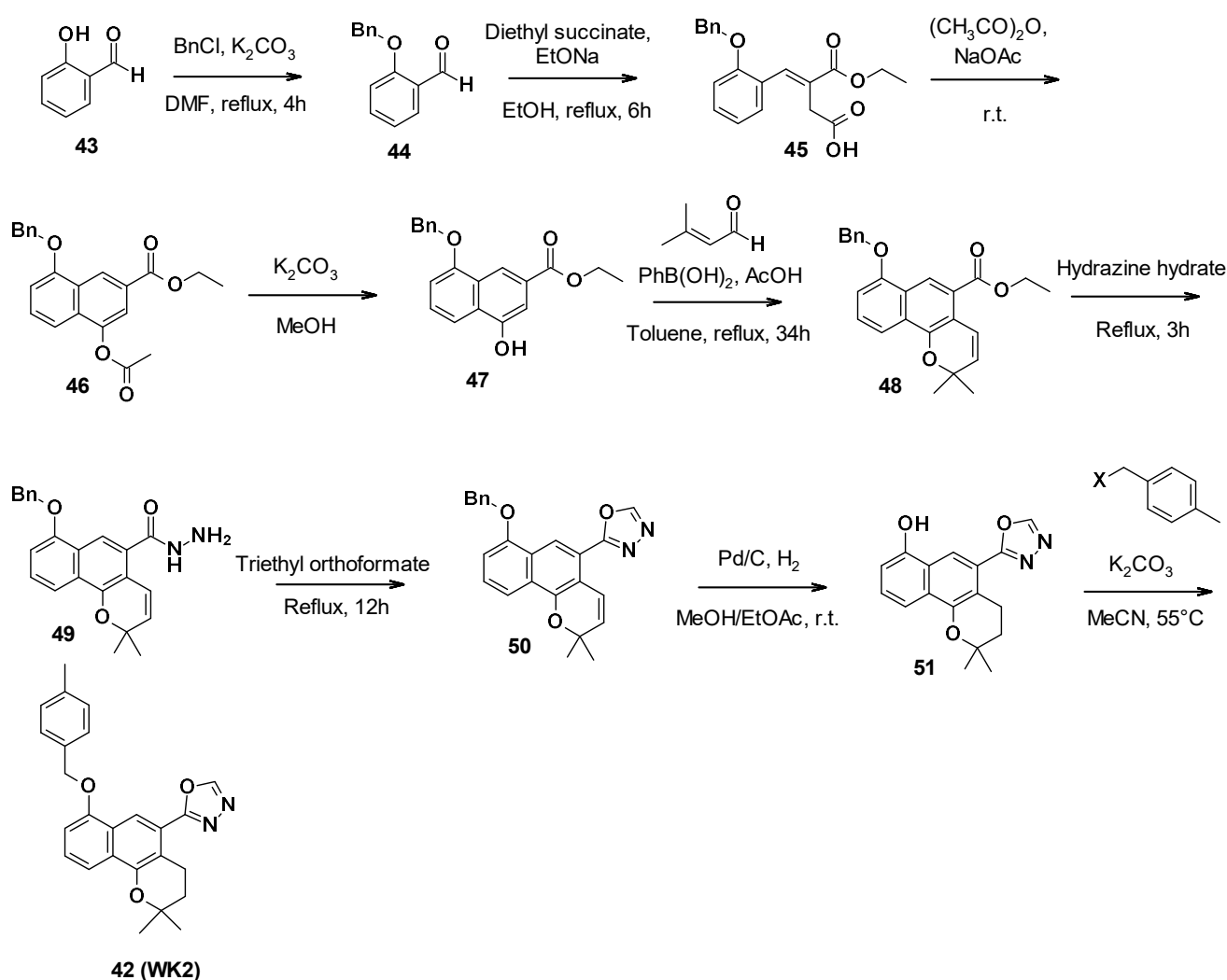
Scheme 5. Description of the synthesis pathway leading to compound **WK2** (**42**).

3.5.3. *In Vitro* Activity

Resulting from the SARs study, compound **WK2** substituted by an oxadiazole ring in position C5 showed the best compromise between potency and the ability to boost several antibiotics. Indeed, **WK2** boosted the antibacterial activity of chlorampheni-col, erythromycin, tetraphenylphosphonium (TPP), and levofloxacin more than 4-fold at 128 μg/mL. To note, **WK2** displayed no antibacterial activity on its own and did not influence the MIC of rifampicin. To further confirm that **WK2** directly targeted AcrB, it was

checked that it had no permeabilizing effect on the IM or OM of Gram-negative bacteria at a concentration of 128 μg/mL by assessing the membrane potential using $DiOC_2(3)$ (3,3′-diethyloxacarbocyanine iodide, a fluorescent membrane potential probe) and measuring the rate of hydrolysis of nitrocefin (a chromogenic β-lactam). Finally, it was shown that **WK2** inhibited the efflux of Nile Red, a dye specifically effluxed by AcrB, with complete inhibitory activity at 100 μM [69].

3.5.4. Pharmacological Properties

WK2 showed low cytotoxicity on HepG2 cells (87% viability at 100 μM) [69]. No data were provided on the solubility of this compound; however, its high hydrophobicity may predict low aqueous solubility.

No *in vivo* activity of the 2*H*-benzo[h]chromene derivatives has been reported in the literature yet.

3.6. NSC Series

NSC-33353-derived compounds have been recently described as MFP AcrA inhibitors and were able to boost the activity of antibiotics such as novobiocin and erythromycin. Screening of 1593 compounds (NCS Diversity Set V) at the NCI and the Developmental Therapeutics Program (DTP) in *E. coli* WT led to the identification of seven AcrA inhibitors, including NSC-60339 (Figure 9) [37]. The binding mode of these compounds was more precisely investigated by Darzynkiewicz et al. [75].
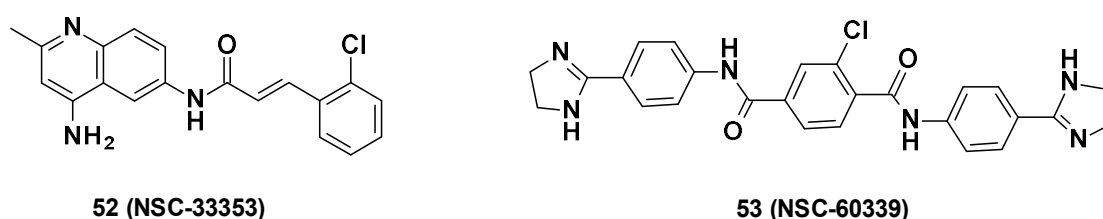

52 (NSC-33353) **53 (NSC-60339)**

Figure 9. Structure of NSC-33353 and NSC-60339.

3.6.1. Structure–Activity Relationships

NSC-33353 (**52**) is a 4,6-diaminoquinoline linked at the C-6 position to a cinnamoyl amide (Figure 9). Previous results showed that the quinoline ring was important for the interaction with AcrA. In order to improve the potency of the compounds, structure–activity relationship studies were performed on the cinnamoyl moiety (Figure 10) [76]:

- **Substitution of cinnamoyl moiety**: First, the substitution of the cinnamoyl group was explored. The introduction of other electron-withdrawing (Cl, Br, NO_2) or electron-donating (isopropyl) groups in position C-2, C-3, or C-4 did not improve the boosting effect of erythromycin (MPC_4 = 3.1–200 μM) and novobiocin (MPC_4 = 6.25–400 μM). Furthermore, these modifications generally led to an increase in the intrinsic antibacterial activity of the compounds.
- **Replacement of cinnamoyl moiety by substituted naphthyl rings**: Because the cinnamoyl moiety was thought to be responsible for the high cytotoxicity of NCS-33353, its replacement with a substituted naphthyl was performed. The introduction of electron-withdrawing (Br, CN, CO_2Me) or electron-donating (OMe) groups at various positions (C-5, C-6, C-7) allowed a slight decrease in cytotoxicity but did not improve the boosting effect of novobiocin and led to compounds no longer able to boost erythromycin. In order to improve the affinity of the inhibitor for AcrA, aromatic substituents were added in C-5 and C-6 positions, but this led to a decrease or even total loss of the boosting effect on erythromycin and novobiocin.
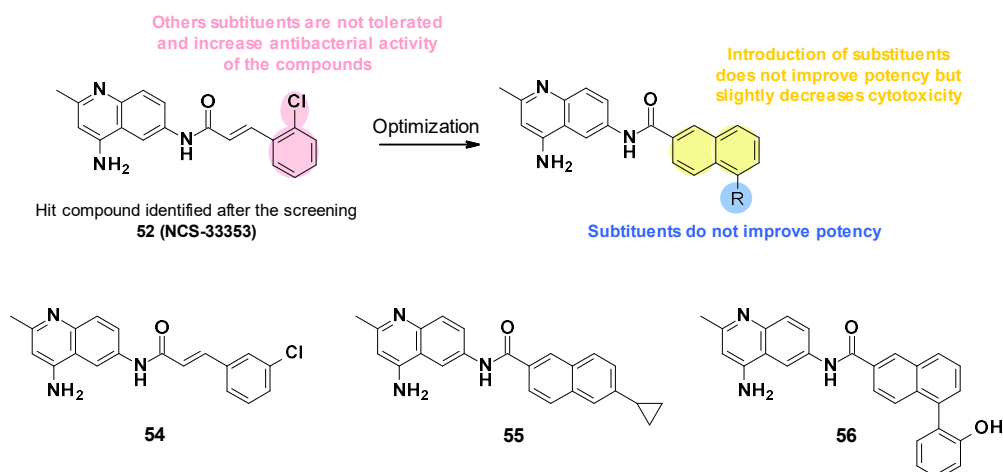
Figure 10. SARs summary and structures of compounds identified after SAR studies.

The SARs allowed the discovery of three compounds (Figure 10).

3.6.2. Chemical Synthesis

NSC-33353 and its analogues were synthesized via a one-step procedure from commercially available 2-methylquinoline-4,6-diamine **57** (Scheme 6) [76]. The synthesis consisted of a selective acylation in the presence of a substituted cinnamoyl chloride or naphthyl chloride. Compounds bearing phenyl on the naphthyl ring were obtained from bromosubstituted naphthyl analogues **60** by the Suzuki reaction.
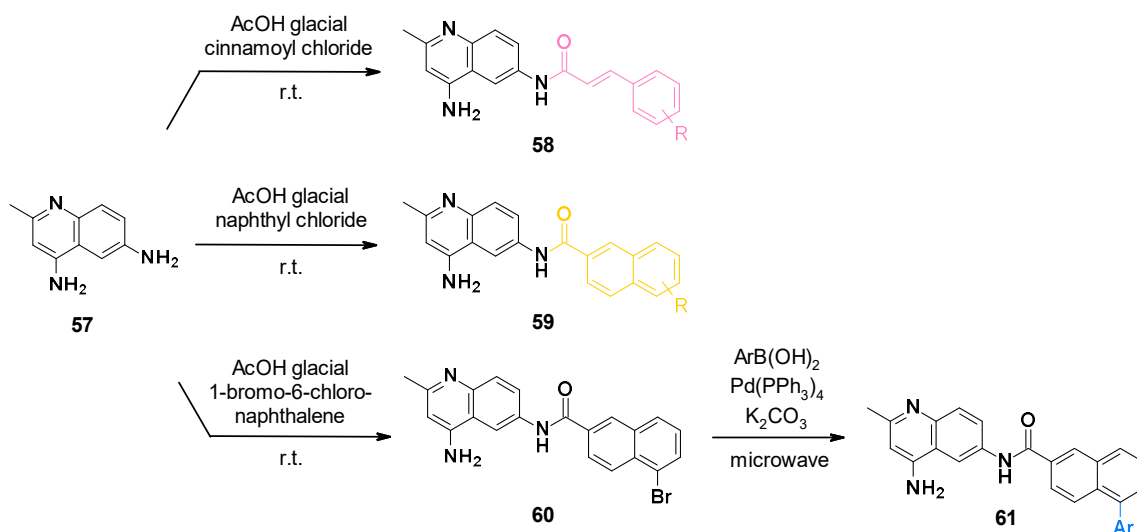
Scheme 6. Chemical synthesis of NSC-33353-derived compounds.

3.6.3. *In Vitro* Activity

NSC-33353 was able to potentiate the activity of novobiocin and erythromycin with an MPC$_4$ of 1.56 and 3.1 μM on *E. coli* [76]. It was reported to have a low antibacterial activity (MIC = 200 μM on *E. coli* WT) but was a substrate of the AcrAB-TolC pump (MIC Δ*tolC* = 12.5 μM).

Cinnamoyl analogues showed higher antibacterial activity on *E. coli* WT (MIC = 25 μM for **54**) than naphthyl analogues (MIC = 200 and 50 μM for **55**, **56**) but also displayed a higher boosting effect of novobiocin and erythromycin than naphthyl analogues [76]. However, the boosting effect observed for compounds **55** and **56** remained less important than for NSC-33353. Noteworthily, NSC-33353 analogues permeabilized the outer membrane and were also substrates of the AcrAB-TolC efflux pump.

Furthermore, NSC-33353 potentiated the activity of erythromycin and novobiocin on other Enterobacterales such as *Enterobacter cloacae* (MPC_4 of 12.5 μM for NOV and ERY) and *K. pneumoniae* (MPC_4 of 12.5 μM for NOV). Conversely, no effect was observed on *P. aeruginosa* [76].

3.6.4. Mode of Action

In surface plasmon resonance assays with purified AcrA, it was shown that all cinnamoyl analogues bound to AcrA with a K_D of 0.02 to 0.3 mM. In contrast, the naphthyl analogues bound to AcrA with different affinities (K_D of 0.001 to 1.18 mM) [76].

Docking studies showed that NSC-33535 bound to site III of AcrA within the AcrAB-TolC complex. This site is adjacent to AcrB and faces the AcrB AP [76].

3.6.5. Pharmacological Properties

NSC-33353 showed significant cytotoxicity in A549 cells (CC_{50} = 10.0 μM) [76]. Naphthyl analogues, such as **55** and **56** (CC_{50} = 31.4, 27.3 μM, respectively), are slightly less cytotoxic than cinnamoyl analogues such as **54** (CC_{50} = 10.1 μM) and NSC-33353. No *in vivo* experiment was reported regarding the NCS series.

3.7. TXA Compounds

TXA09155 (**64**) is a compound developed by Taxis Pharmaceuticals to help treat MDR *P. aeruginosa* infections in burn victims or cystic fibrosis patients. They demonstrated its ability to inhibit the efflux of several antibiotics, including fluoroquinolones, tetracyclines, and β-lactams in *P. aeruginosa*.

TXA09155 is a conformationally constrained indole carboxamide derived from TXA01182 (**63**), itself originating from a synthetic screening of various heterocyclic carboxamide compounds stemming from aryl-alkyl diaminopentanamide EPIs such as **62** [77] (Figure 11).
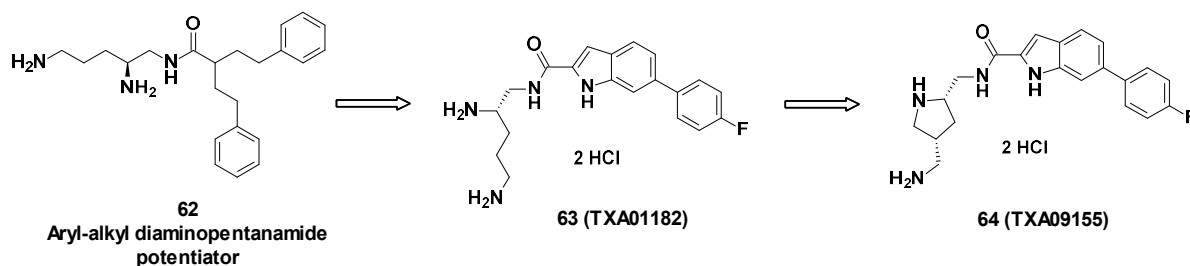

Figure 11. Structure of TXA09155 (**64**), TXA01182 (**63**) and **62**, one of the aryl-alkyl diaminopentanamide potentiators.

3.7.1. Structure–Activity Relationships

The compounds were designed not to cause membrane disruption, in order to avoid toxicity due to non-specific binding. The design was also focused on improving metabolic and serum stability compared to peptidomimetic EPIs. To do so, the aryl-alkyl moiety of the diaminopentanamide potentiators was first replaced with more druggable moieties such as fused heterocycles including benzothiazole, benzimidazole, benzofurane, benzothiophene, indole, and azaindole. These carboxamide-fused heterocycles were linked to a fluorobenzene on one side and a chiral diamine on the other side, yielding TXA01182 [78]. To enhance the potency and improve PK properties, the diamine side chain was conformationally constrained into a pyrrolidine ring, giving TXA09155 [79].

3.7.2. Chemical Synthesis

TXA09155 (**64**) was synthesized in nine steps (Scheme 7). First, commercially available (2*S*-4*R*)-4-hydroxypyrrolidine-2-carboxylic acid was allowed to react with thionyl chloride in methanol to form the corresponding methyl ester **66**. The secondary amine was then protected with benzyl bromide. The free alcohol was activated with tosyl chloride to

perform a nucleophilic substitution with sodium cyanide. Subsequently, the methyl ester was reduced in primary alcohol by lithium borohydride. A Mitsunobu reaction allowed the introduction of the phtalimide, followed by its cleavage with hydrazine to give the corresponding primary amine **72**. This amine could then be involved in a coupling reaction with 6-(4-fluorophenyl)-1*H*-indole-2-carboxylic acid (**73**). The amide derivative finally underwent a reduction step and a deprotection step, followed by the addition of hydrochloric acid to yield TXA09155 [79].
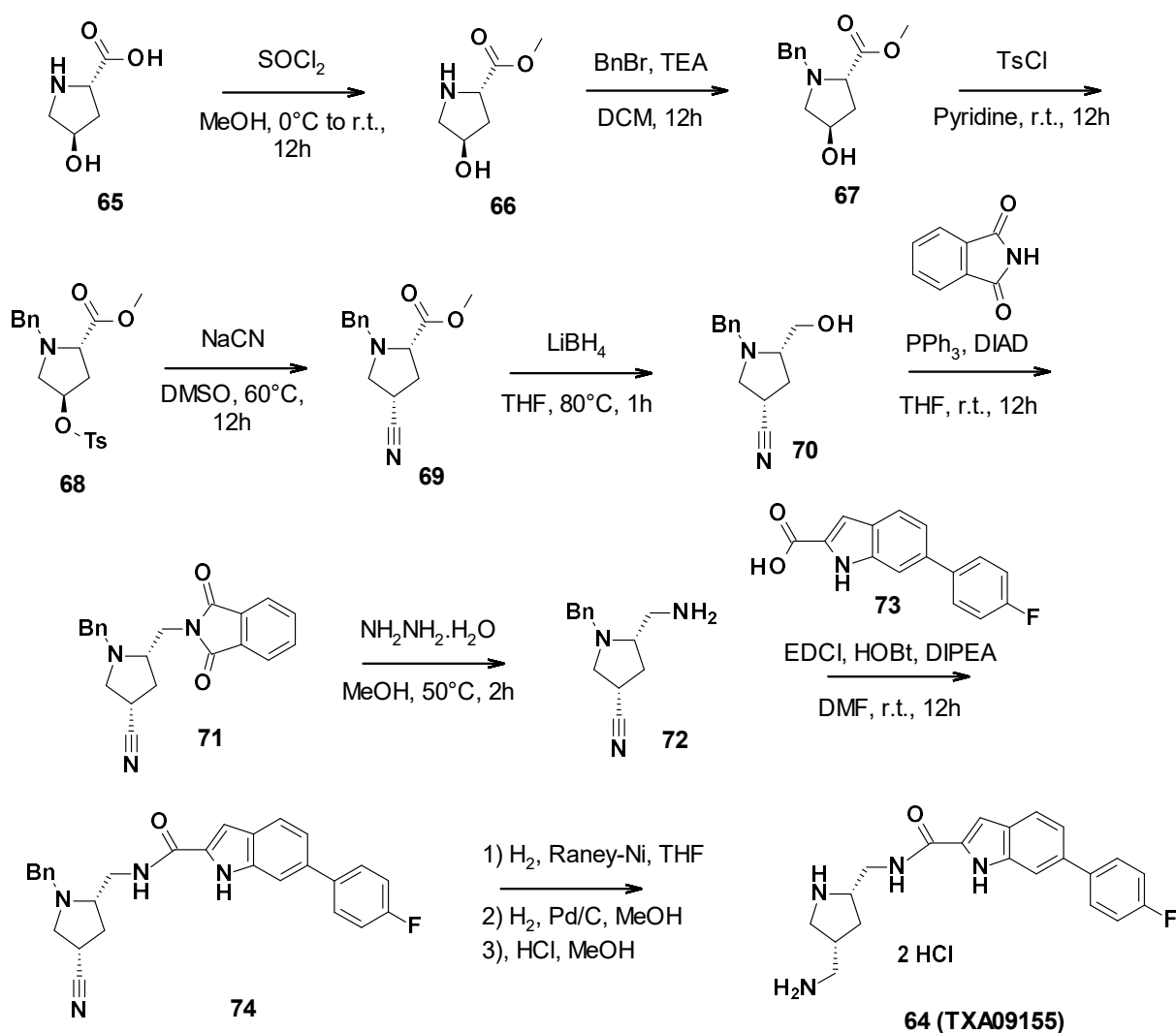
Scheme 7. Description of the synthesis pathway leading to TXA09155 (**64**).

3.7.3. *In Vitro* Activity

Before assessing the potency of TXA09155 on various *P. aeruginosa* strains, its ability to inhibit the efflux of several antibiotics was confirmed. First, inner membrane permeabilization was measured using a flow cytometry-based propidium iodide assay and a nitrocefin assay was performed to monitor outer membrane permeabilization. In these two experiments, TXA09155 did not show significant membrane disruption at concentrations below 50 μg/mL. Then, it was demonstrated that TXA09155 inhibited the efflux of ethidium and levofloxacin. Lastly, TXA09155 did not affect the extent of the proton motive force and did not deplete ATP levels in *P. aeruginosa*, attesting that this compound is able to potentiate antibiotics by blocking their efflux.

Furthermore, the compound's ability to boost antibiotics was tested on *P. aeruginosa* strains overexpressing MexAB-OprM or MexYZ-OprM, two RND-type efflux pumps.

TXA09155 potentiated both cefpirome (third-generation cephalosporin) and levofloxacin by 8-fold. These results were confirmed on a panel of MDR *P. aeruginosa* clinical isolates: TXA09155 was able to lower the percentage of levofloxacin-resistant strains from 85% to 35%. Finally, TXA09155 reduced the frequency of resistance to levofloxacin by more than 149-fold, thus illustrating a further potential benefit of inhibiting efflux in bacteria [79].

Interestingly, the activity of co-trimoxazole, doxycycline, minocycline, and chloramphenicol was also potentiated by TXA09155 in Δ*oprM* strains.

The mode of action of TXA09155 was further explored with the selection of *P. aeruginosa* strains resistant to TXA09155 alone or to the combination of TXA09155/levofloxacin. Strains selected after incubation with TXA09155 alone possessed single-point mutations in the *phoQ* gene or a deletion in the *ompH* gene. *phoQ* codes for a component of the PhoP-PhoQ system, which regulates the expression of more than 100 genes in *P. aeruginosa*, including *mexX*. The deletion of *ompH* has been associated with hypersusceptibility to various antibiotics such as levofloxacin or doxycycline [80]. Hence, Zhang et al. hypothesized that OmpH could be implicated in the correct folding of efflux pumps [81], and in consequence, a deletion in *ompH* could provoke a misfolding of an efflux pump targeted by TXA09155 or TXA09155 could directly target OmpH, resulting in misfolded efflux pump components. On the other hand, strains selected after incubation with the combination of TXA09155/levofloxacine were characterized by a single point mutation in *trpS*, a gene coding for a tryptophan-tRNA ligase, further corroborating the implication of TXA09155 in protein synthesis inhibition as a secondary mode of action [79].

3.7.4. Pharmacological Properties

TXA09155 showed favorable *in vitro* ADME properties: It is highly soluble (>155 μM at physiological pH) and relatively stable in human and rat liver microsomes. Nonetheless, it has shown inhibitory activity on cytochrome P450 3A4 (CYP3A4, IC_{50} = 28.5 μM) and hERG (IC_{50} = 16 μM), suggesting that this compound needs further optimization [79]. Indeed, CYP3A4 catalyzes reactions involved in drug metabolism, and its inhibition can lead to drug–drug interactions, while hERG inhibition can cause heart arrhythmias.

3.7.5. *In Vivo* Activity

No *in vivo* experiment was published regarding TXA09155. However, a compound from the same chemical series (**75**, Figure 12) was tested in a murine septicemia model of infection by *P. aeruginosa*. The combination **75** (3.0 mg/mL bid)/cefepime (10 mg/mL) allowed 100% of the mice to survive at 72 h, whereas cefepime alone only showed 25% survival at 72 h [82].
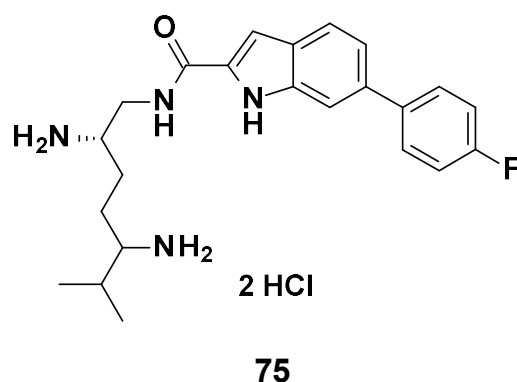

Figure 12. Structure of compound **75**, evaluated *in vivo*.

3.8. Pyridylpiperazines (BDM Compounds)

Pyridylpiperazine compounds have been recently described as AcrB inhibitors and are able to boost antibiotic activity in *E. coli* [83]. BDM88855 (**78**) and derivatives act as allosteric efflux-pump inhibitors, which uniquely bind to the transmembrane domain

of AcrB. This series was discovered by phenotypic screening of a 1280 fragment-library on *E. coli* BW25113 in combination with a sub-active dose of pyridomycin, a compound particularly effluxed by AcrAB-TolC.

3.8.1. Structure-Activity Relationships

BDM73185 (**76**), the hit compound identified from the fragment screening, is a small molecule with a pyridine core substituted by two electron-withdrawing substituents (Cl and CF$_3$) in C-3 and C-5 positions and a basic piperazine moiety in the C-2 position (Figure 13). To improve the potency of BDM73185, structure–activity relationships were performed on the piperazine ring, the trifluoromethyl group, the pyridine moiety, and the chlorine atom [83]:

- **Modification of the piperazine moiety:** Replacement by morpholine or piperidine led to a total loss of activity (EC$_{90}$ > 500 µM) suggesting that the basic nitrogen was important for potency. In addition, the substitution of the amine with methyl led to a 6-fold decrease in potency.
- **Replacement of the trifluoromethyl group**: Substitution with a more polar group (OMe) led to a decrease in potency in contrast to the introduction of hydrophobic substituents. The introduction of halogen atoms was preferred and led to a 5-fold improvement of potency for the compound bearing an iodine atom (**77**, EC$_{90}$ = 12 µM).
- **Replacement of the pyridine core**: Replacement with a quinoline core led to a 15-fold more potent compound (**78**, EC$_{90}$ = 3.4 µM).
- **Replacement of the chlorine atom**: Removal of the chlorine atom led to a significant decrease in potency (EC$_{90}$ > 250 µM), while replacement with other halogen atoms (Br, I) led to a slight improvement in potency (EC$_{90}$ = 1.5 µM and 3 µM, respectively).
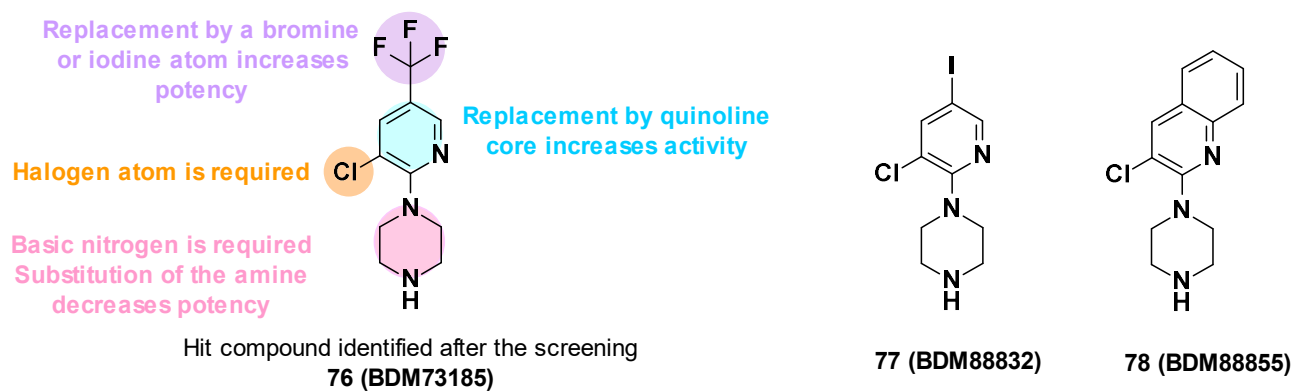
Figure 13. Summary of the SARs performed on BDM73185 (**76**) and structures of BDM88832 (**77**) and BDM88855 (**78**).

The SARs allowed the identification of different compounds such as BDM88832 (**77**) and BDM88855 (**78**), which were 5 to 18 times more potent than the hit BDM73185 (Figure 13) [83].

3.8.2. Chemical Synthesis

BDM88855 (**78**) was synthesized in two steps starting from 2,3-dichloroquinoline (Scheme 8) [83]. Firstly, aromatic nucleophilic substitution was performed with Boc-piperazine. The Boc group was then cleaved by hydrochloric acid in dioxane to afford BDM88855.
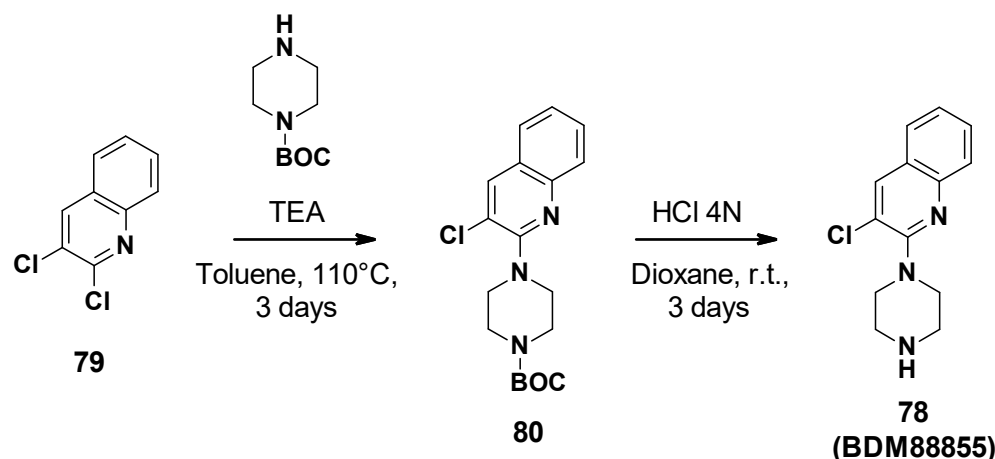
Scheme 8. Description of the synthesis pathway leading to BDM88855 (**78**).

3.8.3. *In Vitro* Activity

Pyridylpiperazine compounds did not exhibit antibacterial activity (MIC$_{90}$ > 250 μM) [83].

At 300 μM, BDM73185 boosted the antibiotic activity of a panel of AcrAB-TolC substrates such as chloramphenicol (8-fold), pyridomycin (4-fold), tetracycline (4-fold), erythromycin, and ciprofloxacin (2-fold), but no effect was observed with non-AcrB substrates such as streptomycin and kanamycin. Moreover, it had no boosting effect on *E. coli* Δ*acrB*, Δ*acrA*, or Δ*tolC* mutants [83].

BDM88855.HCl (100 μM) was also able to boost all the AcrB substrates antibiotics: Oxacillin (>30-fold), linezolid (>30-fold), novobiocin (8-fold), and fusidic acid (8-fold) in *E. coli* wild-type, to levels similar to that observed for *E. coli* Δ*acrAB* [83].

3.8.4. Mode of Action

To confirm the mode of action, resistant mutants were selected on *E. coli* in the presence of BDM73185 and erythromycin. Four strains resistant to BDM73185 but not to erythromycin were identified. Whole-genome sequencing revealed a mutation in the *acrB* gene, more specifically in the part coding for transmembrane helix 5, confirming the mechanism of action. The binding site of these compounds was further confirmed with the co-crystal structures of pyridylpiperazine-based inhibitors that were obtained and showed that BDM88855 acts as an allosteric inhibitor binding to the AcrB transmembrane domain (see Section 4.4) [83].

3.8.5. Pharmacological Properties

BDM73185 and BDM88855.HCl showed no cytotoxicity on BALB/3T3 cells (CC$_{50}$ > 100 μM) and have high aqueous solubility (>200 μM in PBS) [83]. To date, no *in vivo* experiment has been reported for pyridylpiperazines.

4. Structural Perspective on AcrB Substrate and Inhibitor Binding

4.1. *E. coli AcrAB-TolC, the Well-Studied Model System*

E. coli AcrAB-TolC is structurally and functionally arguably the best-studied tripartite RND multidrug efflux pump and transports an extraordinarily broad range of substrates [8,21]. Recently, the functional dominance of the constitutively expressed transporter was impressively demonstrated against the background of an efflux-deficient strain in which a total of 35 efflux pumps were deleted [84]. The structure of the AcrAB-TolC complex was elucidated via single-particle cryoelectron microscopy in an asymmetric conformation that presumably represents the active state of the efflux pump (PDB entry: 5O66, [23]). The asymmetric state in which each of the three AcrB protomers adopts a different conformation has been observed in numerous X-ray structures of the AcrB wildtype protein (or variants) and in complex with substrates or inhibitors ([7,8], this review).

Each AcrB protomer can be structurally divided into a funnel domain (FD) important for AcrB trimerization [85,86], a transmembrane domain (TMD) that energizes drug transport under PMF consumption, and a porter domain (PD) that contains the access pocket (AP) and the deep binding pocket (DBP) and mediates substrate reception, recognition, and translocation (see Figure 14a). The individual protomer conformations of AcrB represent different intermediates of a functional rotation cycle, which, in analogy to the F_1F_o-ATPase or/and based on their function, are called loose (L), tight (T), and open (O), or access, binding, and extrusion [87,88]. During functional rotation, the conformation of the FD remains the same, while the PD and the TMD undergo major conformational changes in a coordinated fashion [87–90]. As can be seen by the comparative co-structural analysis in Section 4.2, most substrates either bind to the AP of the L protomer or the DBP of the T protomer. While the AP (between PD subdomains PC1 and PC2) is present in both the L and T conformation, the DBP (between PD subdomains PC1, PN1, and PN2) is exclusively open in the T state (see Figure 14e). The two polyspecific substrate pockets are separated by the switch loop, a small, adaptive module that participates in substrate binding to both pockets [91,92]. In addition to the large AP and DBP, several transient channels have been reported to be involved in the supply of substrates toward these binding pockets. Both channel 1 (CH1), which originates from the TM7/TM8 groove of an L or T intermediate, and CH2 at the lower cleft entrance lead to the AP [89,91–93]. CH3 and CH4, on the other hand, connect the DBP with the central cavity and the TM1/TM2 groove, respectively [94,95]. All pockets and entry channels are closed in the O protomer but this protomer comprises a unique exit gate to allow substrates to leave via the AcrA/TolC conduit.

Within the TMD, the O conformation represents the occluded state in which D408 (and D407) is (are) protonated [96,97]. The TMD consists of 12 TM helices from which the first bundle (TM1-6) connects to PD subdomains PN1 (TM1) and PN2 (TM2) and the second bundle (TM7-12) is connected to the PC1 (TM7) and PC2 (TM8) subdomains. Residues D407, D408 (both TM4), K940 (TM10), and R971 (TM11) in the TMD core are involved in sequential protonation and deprotonation and are central to the energy conversion during functional rotation [8,96]. The transition from the O to the L state opens a water-filled channel on the cytoplasmic side through which the deprotonation of the proton relay network has been postulated [96]. Within the PD, the L state corresponds to a substrate-accessible resting state [23,98,99]. The L-to-T transition is associated with major conformational changes in both the PD and the TMD. Tight substrate binding within the DBP stabilizes the T state, allowing protons from the periplasm to enter the TMD towards the titratable residues D407 and D408. This protonation changes the electrostatics within the TMD and induces the T to O transition, leading to the extrusion of substrates [96,97].

4.2. Substrate Binding

Due to the small number of directly comparable co-structures for other RND-transporters, the comparative structural analysis carried out here is limited to *E. coli* AcrB. A comparison of AcrB substrates reveals a variety of physicochemical properties. The distinction between substrates, non-substrates, or inhibitors is therefore almost impossible on the basis of the differences in their chemical structures. AcrAB-TolC mediates resistance against compounds, which are very small and simple, such as n-hexane, or very large and complex, such as bleomycin [100]. However, dianionic β-lactams [101] and aminoglycoside antibiotics [102] are giving rise to poor or no resistance phenotypes in *E. coli*, respectively. As a common property, substrates and inhibitors of multidrug efflux pumps such as AcrB comprise one or more hydrophobic (often aromatic) moieties [103–105].

Known *E. coli* AcrB wildtype/substrate and inhibitor co-structures were analyzed for potential protein ligand interactions. All residues within a radius of 3.5 Å around the ligand including its hydrogen atoms were recorded in the PDB structures and assigned to the residues of AcrB. Emerging patterns are shown in Table S1 in Supplementary Materials. It should be noted that within this simplified view, a relative positional relationship does not necessarily indicate a relevant biophysical interaction. Furthermore, the available

high-resolution data indicate the structural importance of structural water molecules. More detailed information can be found in the respective publications [66,92,106]. However, even considering these limitations, some common binding patterns can be observed.
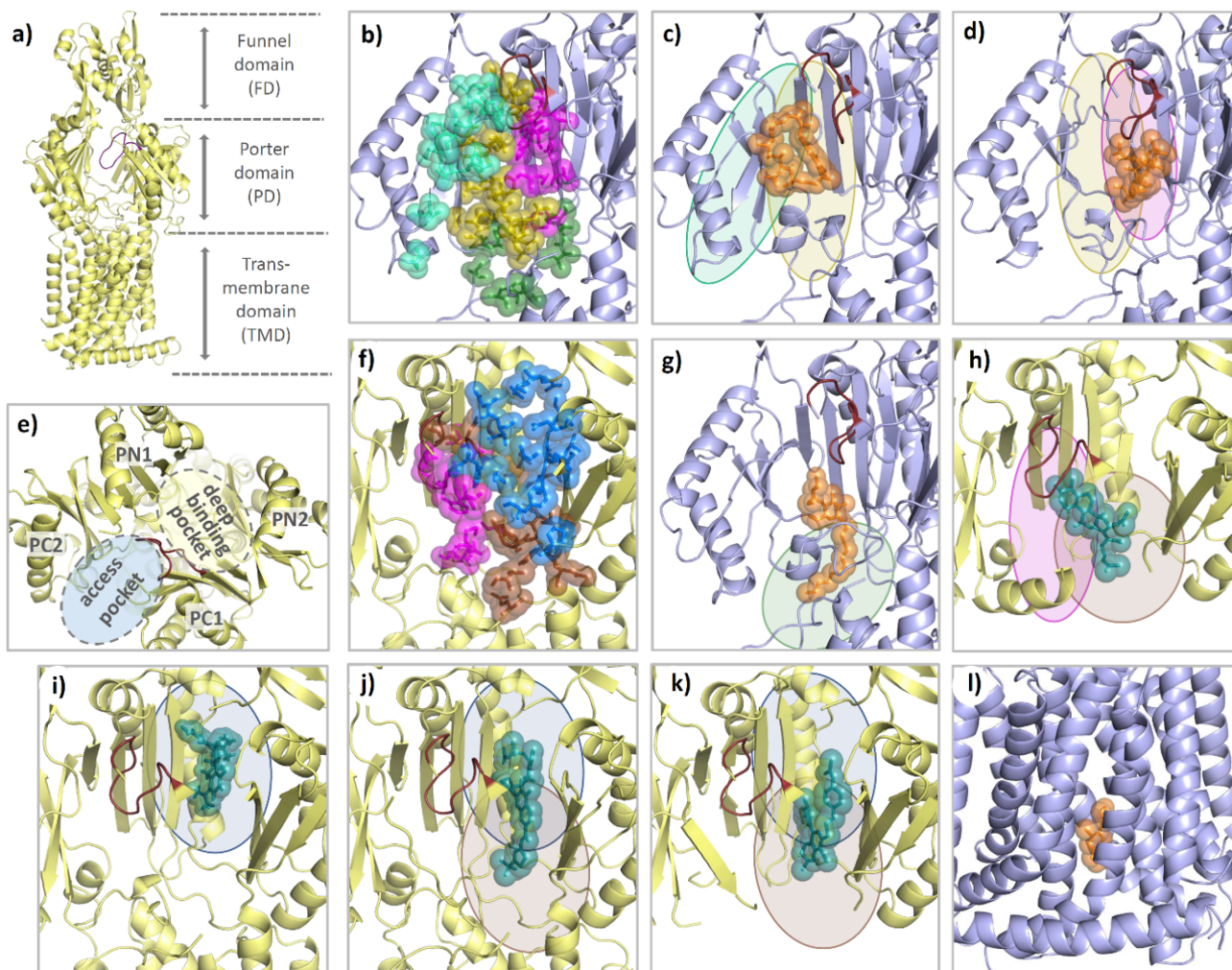

Figure 14. Comparison of the binding modes of AcrB substrates and inhibitors. Each AcrB protomer consists of a funnel domain (FD), a porter domain (PD), and a transmembrane domain (TMD) (**a**). The conformational states loose (L) and tight (T) are indicated by the color of the cartoon representation (light blue and yellow). As can be seen from a top perspective (**e**), the PD of the T protomer contains an access pocket (AP) and a deep binding pocket (DBP) that are separated by the switch loop (ruby). For the L protomer, all residues within 3.5 Å of a ligand are shown as colored spheres from a side perspective through the (removed) PC1 subdomain. Binding residues are grouped into an outer AP (cyan), an inner AP (olive), an AP–DBP interface (magenta), and channel 1 (CH1) (green) (**b**). As highlighted with the colors of the respective binding areas, the 3-formyl-rifamycin molecule (6ZOB) (shown as orange spheres, (**c**)), which is stalled in front of the switch loop, predominantly binds to the outer and inner AP. Erythromycin (3AOC) (**d**), which is located underneath the switch loop, is in close contact with the inner AP and the AP-DBP interface. DDM (6ZOA) was found in CH1 of an L/T intermediate (**g**). Main residues involved in T protomer substrate/inhibitor binding were grouped into an upper DBP groove region (blue), a lower DBP cave region (brown), and the residues of the AP–DBP interface (magenta) (**f**). While the binding of substrates (shown as teal spheres) such as fusidic acid (7B8S) (**h**) and minocycline (4DX5) (**i**) appears to focus on one of the two regions (and part of the AP-DBP interface), inhibitors such as D13-9001 (3W9H) (**j**) and MBX3132 (5ENQ) (**k**) interact strongly with both cave and groove of the DBP. The inhibitor BDM88855 (7OUK) (**l**) binds to a cytoplasmic pocket within the TMD of an early L/T intermediate.

In the AcrB L state, molecules such as rifampicin (PDB entry: 3AOB and 3AOD, [91]), 3-formyl-rifamycin (6ZOB, [93]), and the two stacked doxorubicin molecules (4DX7, [92]) predominantly interact with the outer and inner access pocket (part of the entry tunnel CH2) and to a lesser extent with the AP-DBP interface towards the (closed) deep binding pocket (see Figure 14c and Table S1 in Supplementary Materials). The macrolide antibiotic erythromycin apparently binds particularly strongly to the inner AP and the AP–DBP interface, but also has interactions with the DBP cave region (see Figure 14d). Another channel leading to the AP and DBP is CH1. It originates inside the TM7/TM8 groove. CH1 was suggested to be relevant for the uptake of smaller compounds such as β-lactams [93,107], phenicols, dodecyl β-D-maltoside (DDM), linezolid, and novobiocin [93]. DDM, a validated AcrB substrate, not only binds to the TM7/TM8 groove of AcrB [92,108], but has been recently co-crystallized in an L/T state in which DDM was bound to residues of the AP and the AP-DBP interface (6ZOA, [93]). This detergent was effectively clamped by residues of CH1 including I38, A39, P40, T463, F563, G675, Q865, E866, and S869 (see Figure 14g). The T protomer, in contrast to the L protomer, is characterized by its fully open DBP. In the T protomer, puromycin was found in an intermediate position interacting predominantly with the AP-DBP interface and the DBP cave but also with the DBP groove region and the AP (5NC5, [23]). Binding of fusidic acid, on the other hand, was more focused to the DBP cave and the AP-DBP interface region (see Figure 14h) (7B8S, [106]). In addition to the AP–DBP interface and the DBP cave region, rhodamine 6G (5ENS, [66]) and doxycycline (7B8R, [106], one out of two simultaneously bound molecules) share substantial contacts with the DBP groove. Levofloxacin (7B8T, [106]) and doxorubicin (4DX7, [92]) bind in the DBP cave and groove region while minocycline (2DRD [88], 3AOD, [91], 4DX5, [92] and 5ENT, [66]) and the second (of two simultaneously bound) doxycycline molecules (7B8R, [106]) interact almost exclusively with the DBP groove (see Figure 14i). In addition to co-structures of antibiotics to the periplasmic porter domain, fusidic acid co-structures (5JMN, [109] and 6ZOD, [93]) show simultaneous binding of three fusidic acid molecules to the T protomer transmembrane domain (TMD). One binding site is located at the TM1/TM2 groove at the entrance of CH4, and one molecule binds to the lower part of the TM7/TM8 groove at the entrance of CH1. A third molecule binds deeply into the TMD upon a conformational shift of TM11 and TM12 [93]. This co-structure with multiple bound fusidic acid molecules potentially represents an intermediate stage of transport and/or allosteric modulation sites.

4.3. Competitive Inhibitor Binding

Until the discovery of the BDM series of inhibitors, which bind to the TMD of AcrB (see below) [83], the only RND multidrug efflux pump inhibitors that could be structurally elucidated were bound to the DBP. As shown in Table S1 in Supplementary Materials and Figure 14j,k, D13-9001 (3W9H, [55]) and the MBX series (MBX2329 (5ENO), MBX2931 (5ENP), MBX3132 (5ENQ), and MBX3135 (5ENR), [66]) essentially interact with the entire hydrophobic interaction face of the DBP. These include the DBP cave residues F136, Y327, and F628, as well as the groove residues F178 I277, A279, F610, V612, and F615. Consequently, inhibitor binding appears to differ from substrate binding in terms of the intensity and multiplicity of interactions. The interactions with the DBP region known as the hydrophobic trap (HT) include intense π-π stacking between the planar inhibitor backbones and the aromatic side chains of F178, F615, and F628 [66]. The hydrophobic (and aromatic) character of this DBP region also appears to be present in other (major) RND multidrug efflux pumps [105]. Inhibitors of the MBX series are also in contact with the AP–DBP-interface (M573, F617). Of note, the interactions are extended by the hydrogen bonding interaction of the inhibitors with the side chains Q151, S155, and Q176 and the carbonyl backbone oxygen of A286, which all coordinate water molecules, and in contact with the MBX inhibitor [66].

As a common mode of competitive inhibition, it is assumed that high-affinity interactions between the inhibitor molecules and the DBP prevent substrate binding via steric hinderance. In addition, inhibitor binding to the T state likely prevents the T-O transition,

which presumably arrests the conformation change of the other protomers [66]. The latter assumption is supported by data on structural dynamics of AcrB in the presence of PAβN [110]. In principle, docking and molecular dynamic simulations indicate a similar mode of action for further inhibitors acting in the region of the substrate binding pockets [110–115]. Potent efflux pump inhibitors are therefore likely to fit perfectly into the target binding pocket, which also involves strong interactions with the HT. The simple fact that substrates as such are not permanently bound but are actively transported [116] implies that compared to inhibitor binding, substrate recognition is significantly more flexible and dynamic. Moreover, substitutional analysis of side chains inside binding pockets has revealed substantial resilience of the binding pockets upon change including retaining wildtype resistance phenotypes [8,91,93,106,117]. It appears obvious that the distinction between a substrate and a competitive inhibitor is gradual and strongly dependent on the properties of the respective efflux pump(s). For example, berberine, an excellent substrate of *E. coli* AcrB-TolC [100], inhibits the MexXY-OprM efflux pump from *P. aeruginosa* [118]. Therefore, competitive inhibition in the case of polyspecific efflux pumps remains a complicated field of research, and alternative efflux pump inhibitors with an allosteric mode of action have been recently reported as a promising avenue for the inactivation of RND efflux pumps [83].

4.4. Allosteric Inhibitors Affecting Proton Coupling

The pyridylpiperazine-based inhibitor BDM88855 was resolved within the AcrB transmembrane domain bound to an (partially) induced binding pocket, close to the titratable residues D407, D408, K940, and R971, which are responsible for the translocation of protons, the essential second substrate of RND multidrug efflux pumps [83,119–121]. In the apo protein L state (but not in the T or O state), the titratable residues D407 and D408 within the TMD core are accessible from the cytoplasm [92]. However, the resulting water-filled pocket is not large enough to accommodate the BDM88855 molecule (see Figure 15b). Instead, BDM88855 binds to an alternative L state, in which the transmembrane helices, particularly those of the second repeat (TMs 7-12), are shifted, thereby enlarging the cytoplasmic binding pocket. The situation within the TMD might represent an L-T intermediate (see Figure 15b,c), The periplasmic domain, however, remains in the native L state (see Figure 15a). Accordingly, BDM88855 binding might arrest the L-T transition, which is believed to be a vital process involving major TMD rearrangements, at an early stage [83].

From a structural point of view, the analogy with inhibitor binding to the mycolic acid transporter MmpL3 from *M. tuberculosis* is striking. Although the structure and function of the periplasmic domains of AcrB and MmpL3 differ greatly, their homologous TMDs allow for structural comparison. Monomeric MmpL3 was crystallized in the presence of several anti-tuberculosis MmpL3 inhibitors, all bound to the (putative) proton relay network. The nature and position of the residues involved in this network show a strong analogy to those in AcrB (see Figure 16a). Similar shifts within the MmpL3 TMD between the unbound and the inhibitor-bound states suggest a comparable mode of inhibition for AcrB inhibitor BDM88855 and the MmpL3 inhibitors SQ109 (6AJG), AU1235 (6AJH), ICA38 (6AJJ) [122], NITD-349 (7C2M), and SPIRO (7C2N) [123], (see Figure 16b,c). Interestingly, rimonabant (6AJI) binds to a conformation that essentially corresponds to the native (6AJF, [122]) reference structure of MmpL3, and therefore seems not to induce the TMD shifts as seen in the co-structures for the other MmpL3 inhibitors.

From a structural point of view, considering the high level of conservation within the TMD centers of RND multidrug efflux pumps [105], compounds such as BDM88855 appear to be a versatile alternative or complement to "classical" DBP-based inhibition approaches. In fact, combining approaches could be a more sustainable solution, as both DBP- and TMD-based inhibition strategies on their own appear vulnerable to single amino acid alterations [55,83,124,125].
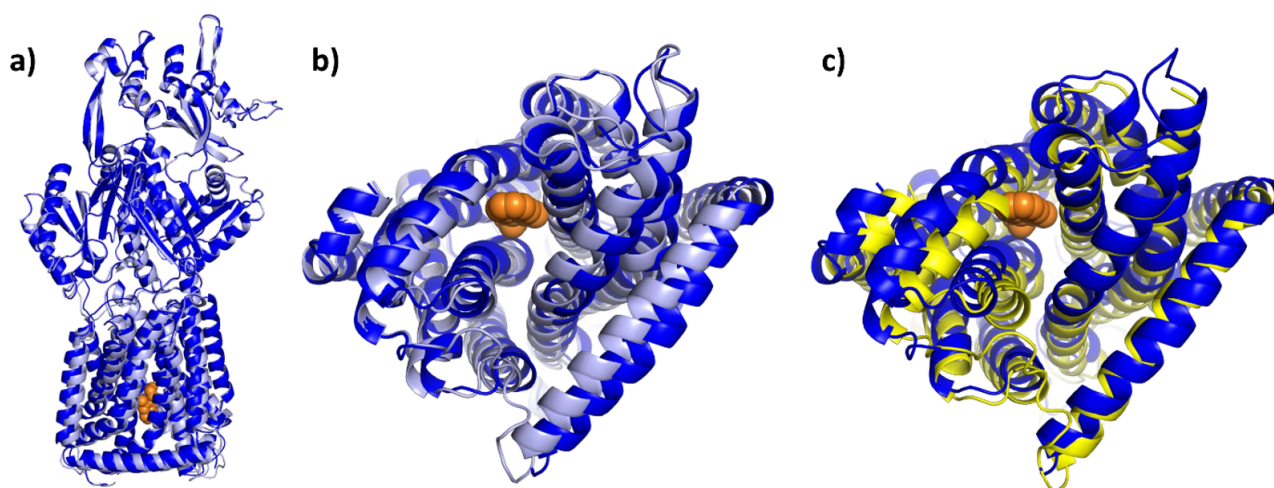
Figure 15. BDM88855-bound intermediate in comparison to the native AcrB L and T state. Cartoon models of the BDM88855 (shown as orange spheres) bound L-state (7OUK) and the native L and T states of AcrB (both 4DX5) were overlayed via their FD domains (residues 181–272 and 724–812). As can be seen, the entire periplasmic domain of AcrB/BDM88855 (blue) remains in the native L state (light blue) (**a**), while there are significant changes in the TMD (**b**). These changes are particularly evident in shifts of the second (right) TMD repeat (helices 7–12), which increases the cytoplasmic pocket. The conformation of the second repeat in the inhibitor-bound structure most closely resembles that of the native T state shown in yellow (**c**).
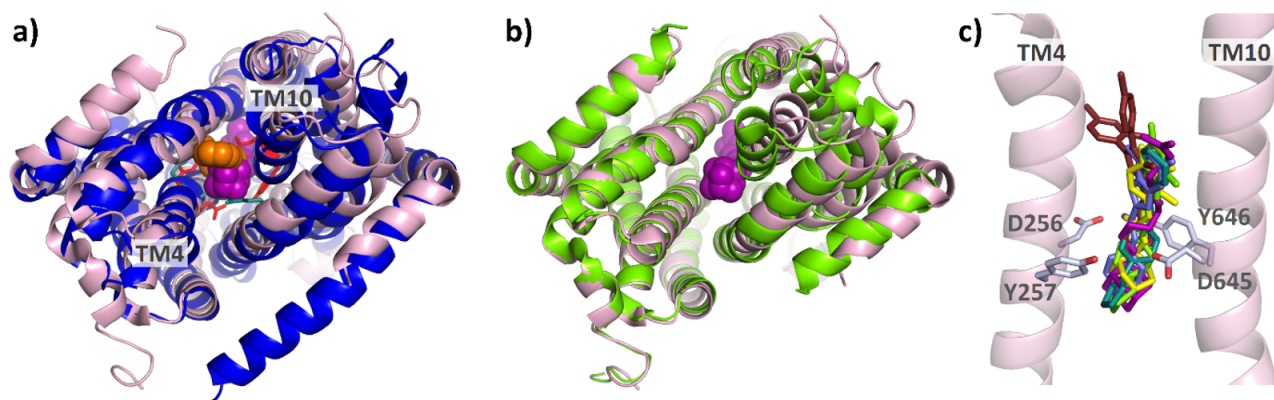

Figure 16. Comparison of AcrB/BDM88855 and inhibitor-bound co-structures of MmpL3: As can be seen from the bottom view (**a**) on the overlayed TMDs of AcrB/BDM88855 (7OUK) (blue/orange) and MmpL3/SQ109 (6AJG) (pink/magenta), both inhibitors bind to comparable areas within the respective proton relay networks (cyan and red sticks). A comparison of the inhibitor-bound MmpL3 co-structure and the native structure (6AJF) (green) shows that inhibition of MmpL3 is also associated with lateral shifts of the TMD repeats (**b**). The effects of MmpL3 inhibitors SQ109 (6AJG) (magenta), AU1235 (6AJH) (yellow), ICA38 (6AJJ) (light green), NITD-349 (7C2M) (light blue), SPIRO (7C2N) (teal), and rimonabant (6AJI) (brown) are likely all based on the disruption of the two Asp-Tyr pairs (D256, Y646 and D645, Y257) (**c**).

5. Conclusions

Efflux pump inhibitors have the potential to greatly assist in the fight against antimicrobial drug resistance. Indeed, the multiple roles of efflux pumps in bacterial resistance (antibiotics efflux, biofilm formation, cell-to-cell communication, pathogenicity, and virulence [32–35]) make them a valuable molecular target.

In this review, we provided an overview of the development of eight classes of EPIs, each able to boost one or more antibiotics in Gram-negative bacteria, from their

discovery to their biological evaluation, as well as their mechanisms of inhibition and binding mode based on co-crystallographic structures and molecular dynamics simulations. The increasing chemical diversity of these EPIs, coupled with their function through the exploitation of different binding pockets, are very promising developments that will increase the chances of bringing EPI to the clinical phase. There are scarce *in vivo* data on the usefulness of the described EPIs, which can be explained by toxicity issues (cell toxicity for PAβN [40], off-target issue for NMP [54]), or a limited range of *in vivo* potency (MBX compounds [67], D13-9001 [62]). EPIs are usually active against one or more efflux pumps from different Enterobacteriaceae (PaβN, NMP, NCS, D13-9001, MBX, BDM), whereas some also have an extended activity spectrum toward *P. aeruginosa* and/or *A. baumannii* (PaβN, NMP, D13-9001, and TXA). *in vivo* data on the EPI resilience toward mutations that render the efflux pumps active but insensitive to EPIs are not documented.

Additionally, the question of clinical bacterial strains characterized by multiple resistance mechanisms (efflux pumps and expression of β-lactamases for example) still needs to be addressed. Regarding this co-occurrence of multidrug efflux and another specific resistance mechanism, it would be conceivable to test antibiotics/EPIs combinations in routine antibiotic susceptibility testing.

Nonetheless, the path is free for a structure-based approach on the basis of efflux pump/EPI co-structures, to develop further and more potent inhibitors. In addition, some EPI series are already well-advanced, such as TXA compounds [79], and new opportunities are arising with the development of allosteric EPIs, such as BDM88855 [83].

Supplementary Materials: The following supporting information can be downloaded at: https://www.mdpi.com/article/10.3390/antibiotics12010180/s1, Table S1: Ligand contacts of known asymmetric AcrB wildtype co-structures. Known asymmetric AcrB wildtype co-structures were analyzed for residues with atoms within 3.5 Å of a substrate or inhibitor in its full atomistic representation (including hydrogen atoms). In addition to the conformational state of the binding protomer (L or T), the protein data bank (PDB) IDs of the respective co-structures are given. Within the co-structures 4DX7 (doxorubicin) and 7B8R (doxycycline) with two substrate molecules bound, each substrate was considered individually. Further ligand–ligand contacts or ligand–water contacts were not taken into consideration.

Author Contributions: Writing—original draft preparation, A.V.D.C., N.C. and R.T.M.; writing—review and editing, A.V.D.C., N.C., R.T.M., R.C.H., M.F. and K.M.P.; funding acquisition, R.C.H., M.F. and K.M.P. All authors have read and agreed to the published version of the manuscript.

Institutional Review Board Statement: Not applicable.

Informed Consent Statement: Not applicable.

Data Availability Statement: Not applicable.

Conflicts of Interest: The authors declare no conflict of interest. The funders had no role in the design of the study; in the collection, analyses, or interpretation of data; in the writing of the manuscript, or in the decision to publish the results.

Abbreviations

AA: Amino acid; ABC: ATP-binding cassette; ADME: Absorption, distribution, metabolism, and excretion; AMR: Antimicrobial resistance; AP: Access pocket; bid: Bis in die, twice a day; Boc: *tert*-butoxycarbonyle; Bn: Benzyle; CC: Cytotoxic concentration; CDI: Carbonyldiimidazole; CFU: Colony Forming Unit; DBP: Deep binding pocket; DCM: Dichloromethane, DDM: Dodecyl β-D-maltoside; DIPEA: N, N-diisopropylethylamine; DMF: N,N-dimethylformamide; DMSO: Dimethylsulfoxide; DTP: Developmental Therapeutics Program; EDCI: 1-ethyl-3-(3-dimethylaminopropyl)carbodiimide; EPI: Efflux pump inhibitor; ERY: Erythromycin; Et: Ethyl, FD: Funnel domain; HLM: Human liver

microsome; HOBt: Hydroxybenzotriazole; HT: Hydrophobic trap; IV: Intravenous; LD: Lethal dose; LPS: Lipopolysaccharides; MATE, Multidrug and toxin extrusion; Me: Methyl; MDR, multidrug resistant; MFP: Membrane fusion protein; MFS: Major facilitator superfamily; MIC: Minimal inhibitory concentration; MLD: Minimum dose causing lethality to $\geq$66% of the animals tested; MLM: Mouse liver microsome; MPC_n: Minimal potentiating concentration by n-fold; MRC: Minimum required concentration; NADPH: Nicotinamide adenine dinucleotide phosphate; NMP: 1-(1-naphtylmethyl)-piperazine; NOV: Novobiocin; OM: Outer membrane; OMF: Outer membrane factor; PAP: Periplasmic adaptor protein; PD: Porter domain; pH: *Potential of Hydrogen*; PK: Pharmacokinetics; PMB: *p*-methoxybenzyl; PMF: Proton motive force; RND: Resistance–nodulation–cell division; r.t.: Room temperature; SAR: Structure–activity relationship; SMR: Small multidrug resistance; TBAF: Tetrabutylammonium fluoride; TCPM: bis(2,4,6-trichlorophenyl)malonate; TEA: Trimethylamine; TFA: Trifluoroacetic acid; THF: Tetrahydrofurane; TMD: Transmembrane domain; Ts: Tosyle; WT: Wild-type.

References

1. Theuretzbacher, U.; Outterson, K.; Engel, A.; Karlén, A. The Global Preclinical Antibacterial Pipeline. *Nat. Rev. Microbiol.* **2020**, *18*, 275–285. [CrossRef]
2. Venter, H. Reversing Resistance to Counter Antimicrobial Resistance in the World Health Organisation's Critical Priority of Most Dangerous Pathogens. *Biosci. Rep.* **2019**, *39*, BSR20180474. [CrossRef] [PubMed]
3. Theuretzbacher, U.; Gottwalt, S.; Beyer, P.; Butler, M.; Czaplewski, L.; Lienhardt, C.; Moja, L.; Paul, M.; Paulin, S.; Rex, J.H.; et al. Analysis of the Clinical Antibacterial and Antituberculosis Pipeline. *Lancet Infect. Dis.* **2019**, *19*, e40–e50. [CrossRef] [PubMed]
4. Ling, L.L.; Schneider, T.; Peoples, A.J.; Spoering, A.L.; Engels, I.; Conlon, B.P.; Mueller, A.; Schäberle, T.F.; Hughes, D.E.; Epstein, S.; et al. A New Antibiotic Kills Pathogens without Detectable Resistance. *Nature* **2015**, *517*, 455–459. [CrossRef]
5. Willyard, C. The Drug-Resistant Bacteria That Pose the Greatest Health Threats. *Nature* **2017**, *543*, 15. [CrossRef] [PubMed]
6. Miller, R.D.; Iinishi, A.; Modaresi, S.M.; Yoo, B.-K.; Curtis, T.D.; Lariviere, P.J.; Liang, L.; Son, S.; Nicolau, S.; Bargabos, R.; et al. Computational Identification of a Systemic Antibiotic for Gram-Negative Bacteria. *Nat. Microbiol.* **2022**, *7*, 1661–1672. [CrossRef]
7. Alav, I.; Kobylka, J.; Kuth, M.S.; Pos, K.M.; Picard, M.; Blair, J.M.A.; Bavro, V.N. Structure, Assembly, and Function of Tripartite Efflux and Type 1 Secretion Systems in Gram-Negative Bacteria. *Chem. Rev.* **2021**, *121*, 5479–5596. [CrossRef]
8. Kobylka, J.; Kuth, M.S.; Müller, R.T.; Geertsma, E.R.; Pos, K.M. AcrB: A Mean, Keen, Drug Efflux Machine. *Ann. N. Y. Acad. Sci.* **2020**, *1459*, 38–68. [CrossRef]
9. Blair, J.M.A.; Richmond, G.E.; Piddock, L.J.V. Multidrug Efflux Pumps in Gram-Negative Bacteria and Their Role in Antibiotic Resistance. *Future Microbiol.* **2014**, *9*, 1165–1177. [CrossRef]
10. Piddock, L.J.V. Clinically Relevant Chromosomally Encoded Multidrug Resistance Efflux Pumps in Bacteria. *Clin. Microbiol. Rev.* **2006**, *19*, 382–402. [CrossRef]
11. Blair, J.M.A.; Webber, M.A.; Baylay, A.J.; Ogbolu, D.O.; Piddock, L.J.V. Molecular Mechanisms of Antibiotic Resistance. *Nat. Rev. Microbiol.* **2015**, *13*, 42–51. [CrossRef]
12. Zgurskaya, H.I.; Walker, J.K.; Parks, J.M.; Rybenkov, V.V. Multidrug Efflux Pumps and the Two-Faced Janus of Substrates and Inhibitors. *Acc. Chem. Res.* **2021**, *54*, 930–939. [CrossRef]
13. Zgurskaya, H.I.; Rybenkov, V.V. Permeability Barriers of Gram-negative Pathogens. *Ann. N. Y. Acad. Sci.* **2020**, *1459*, 5–18. [CrossRef]
14. Bajaj, H.; Acosta Gutierrez, S.; Bodrenko, I.; Malloci, G.; Scorciapino, M.A.; Winterhalter, M.; Ceccarelli, M. Bacterial Outer Membrane Porins as Electrostatic Nanosieves: Exploring Transport Rules of Small Polar Molecules. *ACS Nano* **2017**, *11*, 5465–5473. [CrossRef] [PubMed]
15. Mehla, J.; Malloci, G.; Mansbach, R.; López, C.A.; Tsivkovski, R.; Haynes, K.; Leus, I.V.; Grindstaff, S.B.; Cascella, R.H.; D'Cunha, N.; et al. Predictive Rules of Efflux Inhibition and Avoidance in Pseudomonas Aeruginosa. *Mbio* **2021**, *12*, e02785-20. [CrossRef]
16. El Zahed, S.S.; French, S.; Farha, M.A.; Kumar, G.; Brown, E.D. Physicochemical and Structural Parameters Contributing to the Antibacterial Activity and Efflux Susceptibility of Small-Molecule Inhibitors of Escherichia Coli. *Antimicrob. Agents Chemother.* **2021**, *65*, e01925-20. [CrossRef] [PubMed]
17. Cernicchi, G.; Felicetti, T.; Sabatini, S. Microbial Efflux Pump Inhibitors: A Journey around Quinoline and Indole Derivatives. *Molecules* **2021**, *26*, 6996. [CrossRef]
18. Alenazy, R. Drug Efflux Pump Inhibitors: A Promising Approach to Counter Multidrug Resistance in Gram-Negative Pathogens by Targeting AcrB Protein from AcrAB-TolC Multidrug Efflux Pump from Escherichia Coli. *Biology* **2022**, *11*, 1328. [CrossRef]
19. Seukep, A.J.; Mbuntcha, H.G.; Kuete, V.; Chu, Y.; Fan, E.; Guo, M.-Q. What Approaches to Thwart Bacterial Efflux Pumps-Mediated Resistance? *Antibiotics* **2022**, *11*, 1287. [CrossRef] [PubMed]
20. Ferrer-Espada, R.; Shahrour, H.; Pitts, B.; Stewart, P.S.; Sánchez-Gómez, S.; Martínez-de-Tejada, G. A Permeability-Increasing Drug Synergizes with Bacterial Efflux Pump Inhibitors and Restores Susceptibility to Antibiotics in Multi-Drug Resistant Pseudomonas Aeruginosa Strains. *Sci. Rep.* **2019**, *9*, 3452. [CrossRef] [PubMed]

21. Nikaido, H. RND Transporters in the Living World. *Res. Microbiol.* **2018**, *169*, 363–371. [CrossRef] [PubMed]
22. Du, D.; Wang, Z.; James, N.R.; Voss, J.E.; Klimont, E.; Ohene-Agyei, T.; Venter, H.; Chiu, W.; Luisi, B.F. Structure of the AcrAB–TolC Multidrug Efflux Pump. *Nature* **2014**, *509*, 512–515. [CrossRef]
23. Wang, Z.; Fan, G.; Hryc, C.F.; Blaza, J.N.; Serysheva, I.I.; Schmid, M.F.; Chiu, W.; Luisi, B.F.; Du, D. An Allosteric Transport Mechanism for the AcrAB-TolC Multidrug Efflux Pump. *Elife* **2017**, *6*, e24905. [CrossRef]
24. Glavier, M.; Puvanendran, D.; Salvador, D.; Decossas, M.; Phan, G.; Garnier, C.; Frezza, E.; Cece, Q.; Schoehn, G.; Picard, M.; et al. Antibiotic Export by MexB Multidrug Efflux Transporter Is Allosterically Controlled by a MexA-OprM Chaperone-like Complex. *Nat. Commun.* **2020**, *11*, 4948. [CrossRef]
25. Tsutsumi, K.; Yonehara, R.; Ishizaka-Ikeda, E.; Miyazaki, N.; Maeda, S.; Iwasaki, K.; Nakagawa, A.; Yamashita, E. Structures of the Wild-Type MexAB-OprM Tripartite Pump Reveal Its Complex Formation and Drug Efflux Mechanism. *Nat. Commun.* **2019**, *10*, 1520. [CrossRef] [PubMed]
26. Lamut, A.; Peterlin Mašič, L.; Kikelj, D.; Tomašič, T. Efflux Pump Inhibitors of Clinically Relevant Multidrug Resistant Bacteria. *Med. Res. Rev.* **2019**, *39*, 2460–2504. [CrossRef] [PubMed]
27. Zgurskaya, H.I.; Adamiak, J.W.; Leus, I.V. Making Sense of Drug-Efflux Transporters in the Physiological Environment. *Curr. Opin. Microbiol.* **2022**, *69*, 102179. [CrossRef]
28. Hernando-Amado, S.; Blanco, P.; Alcalde-Rico, M.; Corona, F.; Reales-Calderón, J.A.; Sánchez, M.B.; Martínez, J.L. Multidrug Efflux Pumps as Main Players in Intrinsic and Acquired Resistance to Antimicrobials. *Drug Resist. Updates* **2016**, *28*, 13–27. [CrossRef] [PubMed]
29. Ricci, V.; Tzakas, P.; Buckley, A.; Coldham, N.C.; Piddock, L.J.V. Ciprofloxacin-Resistant *Salmonella Enterica* Serovar Typhimurium Strains Are Difficult To Select in the Absence of AcrB and TolC. *Antimicrob. Agents Chemother.* **2006**, *50*, 38–42. [CrossRef]
30. Nolivos, S.; Cayron, J.; Dedieu, A.; Page, A.; Delolme, F.; Lesterlin, C. Role of AcrAB-TolC Multidrug Efflux Pump in Drug-Resistance Acquisition by Plasmid Transfer. *Science* **2019**, *364*, 778–782. [CrossRef]
31. Pu, Y.; Zhao, Z.; Li, Y.; Zou, J.; Ma, Q.; Zhao, Y.; Ke, Y.; Zhu, Y.; Chen, H.; Baker, M.A.B.; et al. Enhanced Efflux Activity Facilitates Drug Tolerance in Dormant Bacterial Cells. *Mol. Cell* **2016**, *62*, 284–294. [CrossRef] [PubMed]
32. Evans, K.; Passador, L.; Srikumar, R.; Tsang, E.; Nezezon, J.; Poole, K. Influence of the MexAB-OprM Multidrug Efflux System on Quorum Sensing in *Pseudomonas Aeruginosa*. *J. Bacteriol.* **1998**, *180*, 5443–5447. [CrossRef] [PubMed]
33. Aendekerk, S.; Diggle, S.P.; Song, Z.; Høiby, N.; Cornelis, P.; Williams, P.; Cámara, M. The MexGHI-OpmD Multidrug Efflux Pump Controls Growth, Antibiotic Susceptibility and Virulence in Pseudomonas Aeruginosa via 4-Quinolone-Dependent Cell-to-Cell Communication. *Microbiology* **2005**, *151*, 1113–1125. [CrossRef] [PubMed]
34. Alav, I.; Sutton, J.M.; Rahman, K.M. Role of Bacterial Efflux Pumps in Biofilm Formation. *J. Antimicrob. Chemother.* **2018**, *73*, 2003–2020. [CrossRef]
35. Sun, J.; Deng, Z.; Yan, A. Bacterial Multidrug Efflux Pumps: Mechanisms, Physiology and Pharmacological Exploitations. *Biochem. Biophys. Res. Commun.* **2014**, *453*, 254–267. [CrossRef] [PubMed]
36. Jesin, J.A.; Stone, T.A.; Mitchell, C.J.; Reading, E.; Deber, C.M. Peptide-Based Approach to Inhibition of the Multidrug Resistance Efflux Pump AcrB. *Biochemistry* **2020**, *59*, 3973–3981. [CrossRef]
37. Abdali, N.; Parks, J.M.; Haynes, K.M.; Chaney, J.L.; Green, A.T.; Wolloscheck, D.; Walker, J.K.; Rybenkov, V.V.; Baudry, J.; Smith, J.C.; et al. Reviving Antibiotics: Efflux Pump Inhibitors That Interact with AcrA, a Membrane Fusion Protein of the AcrAB-TolC Multidrug Efflux Pump. *ACS Infect. Dis.* **2017**, *3*, 89–98. [CrossRef]
38. Chamberland, S.; Hecker, S.J.; Lee, V.J.; Trias, J. Inhibiteurs de pompe d'efflux. WO 1996033285A1, 19 April 1996.
39. Renau, T.E.; Léger, R.; Flamme, E.M.; Sangalang, J.; She, M.W.; Yen, R.; Gannon, C.L.; Griffith, D.; Chamberland, S.; Lomovskaya, O.; et al. Inhibitors of Efflux Pumps in *Pseudomonas a Eruginosa* Potentiate the Activity of the Fluoroquinolone Antibacterial Levofloxacin. *J. Med. Chem.* **1999**, *42*, 4928–4931. [CrossRef]
40. Lomovskaya, O.; Bostian, K.A. Practical Applications and Feasibility of Efflux Pump Inhibitors in the Clinic—A Vision for Applied Use. *Biochem. Pharmacol.* **2006**, *71*, 910–918. [CrossRef]
41. Lomovskaya, O.; Warren, M.S.; Lee, A.; Galazzo, J.; Fronko, R.; Lee, M.; Blais, J.; Cho, D.; Chamberland, S.; Renau, T.; et al. Identification and Characterization of Inhibitors of Multidrug Resistance Efflux Pumps in *Pseudomonas Aeruginosa*: Novel Agents for Combination Therapy. *Antimicrob. Agents Chemother.* **2001**, *45*, 105–116. [CrossRef] [PubMed]
42. Renau, T.E.; Gannon, C.L.; Mathias, K.M.; Lomovskaya, O.; Chamberland, S.; Lee, V.J.; Ohta, T.; Nakayama, K.; Ishida, Y. Addressing the Stability of C-Capped Dipeptide E,ux Pump Inhibitors That Potentiate the Activity of Levofloxacin In. *Bioorg. Med. Chem. Lett.* **2001**, *5*, 663–667. [CrossRef] [PubMed]
43. Renau, T.E.; Léger, R.; Filonova, L.; Flamme, E.M.; Wang, M.; Yen, R.; Madsen, D.; Griffith, D.; Chamberland, S.; Dudley, M.N.; et al. Conformationally-Restricted Analogues of Efflux Pump Inhibitors That Potentiate the Activity of Levofloxacin in Pseudomonas Aeruginosa. *Bioorganic Med. Chem. Lett.* **2003**, *13*, 2755–2758. [CrossRef]
44. Léger, R.; Yen, R.; She, M.W.; Lee, V.J.; Hecker, S.J. N-Linked Solid Phase Peptide Synthesis. *Tetrahedron Lett.* **1998**, *39*, 4171–4174. [CrossRef]
45. Lamers, R.P.; Cavallari, J.F.; Burrows, L.L. The Efflux Inhibitor Phenylalanine-Arginine Beta-Naphthylamide (PAβN) Permeabilizes the Outer Membrane of Gram-Negative Bacteria. *PLoS ONE* **2013**, *8*, e60666. [CrossRef]

46. Lin, K.-H.; Lo, C.-C.; Chou, M.-C.; Yeh, T.-H.; Chen, K.-L.; Liao, W.-Y.; Lo, H.-R. Synergistic Actions of Benzyl Isothiocyanate with Ethylenediaminetetraacetic Acid and Efflux Pump Inhibitor Phenylalanine-Arginine β-Naphthylamide Against Multidrug-Resistant *Escherichia Coli*. *Microb. Drug Resist.* **2020**, *26*, 468–474. [CrossRef] [PubMed]

47. Cortez-Cordova, J.; Kumar, A. Activity of the Efflux Pump Inhibitor Phenylalanine-Arginine β-Naphthylamide against the AdeFGH Pump of Acinetobacter Baumannii. *Int. J. Antimicrob. Agents* **2011**, *37*, 420–424. [CrossRef]

48. Watkins, W.J.; Landaverry, Y.; Léger, R.; Litman, R.; Renau, T.E.; Williams, N.; Yen, R.; Zhang, J.Z.; Chamberland, S.; Madsen, D.; et al. The Relationship between Physicochemical Properties, *In Vitro* Activity and Pharmacokinetic Profiles of Analogues of Diamine-Containing Efflux Pump Inhibitors. *Bioorganic Med. Chem. Lett.* **2003**, *13*, 4241–4244. [CrossRef]

49. Bohnert, J.A.; Kern, W.V. Selected Arylpiperazines Are Capable of Reversing Multidrug Resistance in *Escherichia Coli* Overexpressing RND Efflux Pumps. *Antimicrob. Agents Chemother.* **2005**, *49*, 849–852. [CrossRef]

50. Chupak, L.S.; Ding, M.; Gentles, R.G.; Huang, Y.; Martin, S.W.; Mcdonald, I.M.; Mercer, S.E.; Olson, R.E.; Velaparthi, U.; Wichroski, M.; et al. Naphthyridinone Compounds Useful as t Cell Activators. WO 2020006016A1, 2 January 2020.

51. Kern, W.V.; Steinke, P.; Schumacher, A.; Schuster, S.; Baum, H.; von Bohnert, J.A. Effect of 1-(1-Naphthylmethyl)-Piperazine, a Novel Putative Efflux Pump Inhibitor, on Antimicrobial Drug Susceptibility in Clinical Isolates of Escherichia Coli. *J. Antimicrob. Chemother.* **2006**, *57*, 339–343. [CrossRef]

52. Schumacher, A.; Steinke, P.; Bohnert, J.A.; Akova, M.; Jonas, D.; Kern, W.V. Effect of 1-(1-Naphthylmethyl)-Piperazine, a Novel Putative Efflux Pump Inhibitor, on Antimicrobial Drug Susceptibility in Clinical Isolates of Enterobacteriaceae Other than Escherichia Coli. *J. Antimicrob. Chemother.* **2006**, *57*, 344–348. [CrossRef] [PubMed]

53. Pannek, S.; Higgins, P.G.; Steinke, P.; Jonas, D.; Akova, M.; Bohnert, J.A.; Seifert, H.; Kern, W.V. Multidrug Efflux Inhibition in Acinetobacter Baumannii: Comparison between 1-(1-Naphthylmethyl)-Piperazine and Phenyl-Arginine-β-Naphthylamide. *J. Antimicrob. Chemother.* **2006**, *57*, 970–974. [CrossRef] [PubMed]

54. Bolla, J.-M.; Alibert-Franco, S.; Handzlik, J.; Chevalier, J.; Mahamoud, A.; Boyer, G.; Kieć-Kononowicz, K.; Pagès, J.-M. Strategies for Bypassing the Membrane Barrier in Multidrug Resistant Gram-Negative Bacteria. *FEBS Lett.* **2011**, *585*, 1682–1690. [CrossRef]

55. Nakashima, R.; Sakurai, K.; Yamasaki, S.; Hayashi, K.; Nagata, C.; Hoshino, K.; Onodera, Y.; Nishino, K.; Yamaguchi, A. Structural Basis for the Inhibition of Bacterial Multidrug Exporters. *Nature* **2013**, *500*, 102–106. [CrossRef]

56. Nakayama, K.; Ishida, Y.; Ohtsuka, M.; Kawato, H.; Yoshida, K.; Yokomizo, Y.; Hosono, S.; Ohta, T.; Hoshino, K.; Ishida, H.; et al. MexAB-OprM-Specific Efflux Pump Inhibitors in Pseudomonas Aeruginosa. Part 1: Discovery and Early Strategies for Lead Optimization. *Bioorganic Med. Chem. Lett.* **2003**, *13*, 4201–4204. [CrossRef] [PubMed]

57. Nakayama, K.; Ishida, Y.; Ohtsuka, M.; Kawato, H.; Yoshida, K.; Yokomizo, Y.; Ohta, T.; Hoshino, K.; Otani, T.; Kurosaka, Y.; et al. MexAB-OprM Specific Efflux Pump Inhibitors in Pseudomonas Aeruginosa. Part 2: Achieving Activity *in vivo* through the Use of Alternative Scaffolds. *Bioorganic Med. Chem. Lett.* **2003**, *13*, 4205–4208. [CrossRef]

58. Nakayama, K.; Kawato, H.; Watanabe, J.; Ohtsuka, M.; Yoshida, K.; Yokomizo, Y.; Sakamoto, A.; Kuru, N.; Ohta, T.; Hoshino, K.; et al. MexAB-OprM Specific Efflux Pump Inhibitors in Pseudomonas Aeruginosa. Part 3: Optimization of Potency in the Pyridopyrimidine Series through the Application of a Pharmacophore Model. *Bioorganic Med. Chem. Lett.* **2004**, *14*, 475–479. [CrossRef]

59. Nakayama, K.; Kuru, N.; Ohtsuka, M.; Yokomizo, Y.; Sakamoto, A.; Kawato, H.; Yoshida, K.; Ohta, T.; Hoshino, K.; Akimoto, K.; et al. MexAB-OprM Specific Efflux Pump Inhibitors in Pseudomonas Aeruginosa. Part 4: Addressing the Problem of Poor Stability Due to Photoisomerization of an Acrylic Acid Moiety. *Bioorganic Med. Chem. Lett.* **2004**, *14*, 2493–2497. [CrossRef]

60. Yoshida, K.; Nakayama, K.; Kuru, N.; Kobayashi, S.; Ohtsuka, M.; Takemura, M.; Hoshino, K.; Kanda, H.; Zhang, J.Z.; Lee, V.J.; et al. MexAB-OprM Specific Efflux Pump Inhibitors in Pseudomonas Aeruginosa. Part 5: Carbon-Substituted Analogues at the C-2 Position. *Bioorganic Med. Chem.* **2006**, *14*, 1993–2004. [CrossRef]

61. Yoshida, K.; Nakayama, K.; Yokomizo, Y.; Ohtsuka, M.; Takemura, M.; Hoshino, K.; Kanda, H.; Namba, K.; Nitanai, H.; Zhang, J.Z.; et al. MexAB-OprM Specific Efflux Pump Inhibitors in Pseudomonas Aeruginosa. Part 6: Exploration of Aromatic Substituents. *Bioorganic Med. Chem.* **2006**, *14*, 8506–8518. [CrossRef]

62. Yoshida, K.; Nakayama, K.; Ohtsuka, M.; Kuru, N.; Yokomizo, Y.; Sakamoto, A.; Takemura, M.; Hoshino, K.; Kanda, H.; Nitanai, H.; et al. MexAB-OprM Specific Efflux Pump Inhibitors in Pseudomonas Aeruginosa. Part 7: Highly Soluble and *in vivo* Active Quaternary Ammonium Analogue D13-9001, a Potential Preclinical Candidate. *Bioorganic Med. Chem.* **2007**, *15*, 7087–7097. [CrossRef] [PubMed]

63. Rathi, E.; Kumar, A.; Kini, S.G. Computational Approaches in Efflux Pump Inhibitors: Current Status and Prospects. *Drug Discov. Today* **2020**, *25*, 1883–1890. [CrossRef] [PubMed]

64. Opperman, T.J.; Kwasny, S.M.; Kim, H.-S.; Nguyen, S.T.; Houseweart, C.; D'Souza, S.; Walker, G.C.; Peet, N.P.; Nikaido, H.; Bowlin, T.L. Characterization of a Novel Pyranopyridine Inhibitor of the AcrAB Efflux Pump of Escherichia Coli. *Antimicrob. Agents Chemother.* **2014**, *58*, 722–733. [CrossRef]

65. Nguyen, S.T.; Kwasny, S.M.; Ding, X.; Cardinale, S.C.; McCarthy, C.T.; Kim, H.-S.; Nikaido, H.; Peet, N.P.; Williams, J.D.; Bowlin, T.L.; et al. Structure–Activity Relationships of a Novel Pyranopyridine Series of Gram-Negative Bacterial Efflux Pump Inhibitors. *Bioorganic Med. Chem.* **2015**, *23*, 2024–2034. [CrossRef]

66. Sjuts, H.; Vargiu, A.V.; Kwasny, S.M.; Nguyen, S.T.; Kim, H.-S.; Ding, X.; Ornik, A.R.; Ruggerone, P.; Bowlin, T.L.; Nikaido, H.; et al. Molecular Basis for Inhibition of AcrB Multidrug Efflux Pump by Novel and Powerful Pyranopyridine Derivatives. *Proc. Natl. Acad. Sci. USA* **2016**, *113*, 3509–3514. [CrossRef] [PubMed]

67. Opperman, T.J.; Kwasny, S.M.; Barber, R.; Cardinale, S.C.; Carter, K.; Pulse, M.; Weiss, W.J.; Bowlin, T.L.; Aron, Z. *In Vivo* Proof of Principle for MBX-4191, A Pyranopyridine Efflux Pump Inhibitor. Poster 564 presented at the American Society of Microbiology (ASM) Microbe 2018 Conference, Atlanta, Georgia, 7–11 June 2018.

68. Moir, D.T.; Opperman, T.J.; Aron, Z.D.; Bowlin, T.L. Adjunctive Therapy for Multidrug-Resistant Bacterial Infections: Type III Secretion System and Efflux Inhibitors. *Drug Discov. Today* **2021**, *26*, 2173–2181. [CrossRef] [PubMed]

69. Wang, Y.; Alenazy, R.; Gu, X.; Polyak, S.W.; Zhang, P.; Sykes, M.J.; Zhang, N.; Venter, H.; Ma, S. Design and Structural Optimization of Novel 2H-Benzo[h]Chromene Derivatives That Target AcrB and Reverse Bacterial Multidrug Resistance. *Eur. J. Med. Chem.* **2021**, *213*, 113049. [CrossRef]

70. Wang, Y.; Mowla, R.; Guo, L.; Ogunniyi, A.D.; Rahman, T.; De Barros Lopes, M.A.; Ma, S.; Venter, H. Evaluation of a Series of 2-Napthamide Derivatives as Inhibitors of the Drug Efflux Pump AcrB for the Reversal of Antimicrobial Resistance. *Bioorganic Med. Chem. Lett.* **2017**, *27*, 733–739. [CrossRef]

71. Wang, Y.; Mowla, R.; Ji, S.; Guo, L.; De Barros Lopes, M.A.; Jin, C.; Song, D.; Ma, S.; Venter, H. Design, Synthesis and Biological Activity Evaluation of Novel 4-Subtituted 2-Naphthamide Derivatives as AcrB Inhibitors. *Eur. J. Med. Chem.* **2018**, *143*, 699–709. [CrossRef]

72. Jin, C.; Alenazy, R.; Wang, Y.; Mowla, R.; Qin, Y.; Tan, J.Q.E.; Modi, N.D.; Gu, X.; Polyak, S.W.; Venter, H.; et al. Design, Synthesis and Evaluation of a Series of 5-Methoxy-2,3-Naphthalimide Derivatives as AcrB Inhibitors for the Reversal of Bacterial Resistance. *Bioorganic Med. Chem. Lett.* **2019**, *29*, 882–889. [CrossRef]

73. Wang, Y.; Alenzy, R.; Song, D.; Liu, X.; Teng, Y.; Mowla, R.; Ma, Y.; Polyak, S.W.; Venter, H.; Ma, S. Structural Optimization of Natural Product Nordihydroguaretic Acid to Discover Novel Analogues as AcrB Inhibitors. *Eur. J. Med. Chem.* **2020**, *186*, 111910. [CrossRef] [PubMed]

74. Ohene-Agyei, T.; Mowla, R.; Rahman, T.; Venter, H. Phytochemicals Increase the Antibacterial Activity of Antibiotics by Acting on a Drug Efflux Pump. *MicrobiologyOpen* **2014**, *3*, 885–896. [CrossRef]

75. Darzynkiewicz, Z.M. Identification of Binding Sites for Efflux Pump Inhibitors of the AcrAB-TolC Component AcrA. *Biophys. J.* **2019**, *116*, 648–658. [CrossRef]

76. D'Cunha, N.; Moniruzzaman, M.; Haynes, K.; Malloci, G.; Cooper, C.J.; Margiotta, E.; Vargiu, A.V.; Uddin, M.R.; Leus, I.V.; Cao, F.; et al. Mechanistic Duality of Bacterial Efflux Substrates and Inhibitors: Example of Simple Substituted Cinnamoyl and Naphthyl Amides. *ACS Infect. Dis.* **2021**, *7*, 2650–2665. [CrossRef]

77. Blankson, G.; Parhi, A.K.; Kaul, M.; Pilch, D.S.; LaVoie, E.J. Structure-Activity Relationships of Potentiators of the Antibiotic Activity of Clarithromycin against Escherichia Coli. *Eur. J. Med. Chem.* **2019**, *178*, 30–38. [CrossRef]

78. Yuan, Y.; Rosado-Lugo, J.D.; Zhang, Y.; Datta, P.; Sun, Y.; Cao, Y.; Banerjee, A.; Parhi, A.K. Evaluation of Heterocyclic Carboxamides as Potential Efflux Pump Inhibitors in Pseudomonas Aeruginosa. *Antibiotics* **2021**, *11*, 30. [CrossRef] [PubMed]

79. Zhang, Y.; Rosado-Lugo, J.D.; Datta, P.; Sun, Y.; Cao, Y.; Banerjee, A.; Yuan, Y.; Parhi, A.K. Evaluation of a Conformationally Constrained Indole Carboxamide as a Potential Efflux Pump Inhibitor in Pseudomonas Aeruginosa. *Antibiotics* **2022**, *11*, 716. [CrossRef] [PubMed]

80. Dötsch, A.; Becker, T.; Pommerenke, C.; Magnowska, Z.; Jänsch, L.; Häussler, S. Genomewide Identification of Genetic Determinants of Antimicrobial Drug Resistance in *Pseudomonas Aeruginosa*. *Antimicrob. Agents Chemother.* **2009**, *53*, 2522–2531. [CrossRef] [PubMed]

81. Hirvas, L.; Coleman, J.; Koski, P.; Vaara, M. Bacterial 'Histone-like Protein I' (HLP-I) Is an Outer Membrane Constituent? *FEBS Lett.* **1990**, *262*, 123–126. [CrossRef]

82. Lavoie, E.J.; Parhi, A.; Yuan, Y.; Zhang, Y.; SUN, Y. Indole Derivatives as Efflux Pump Inhibitors. WO 2018165611A1, 13 September 2018.

83. Plé, C.; Tam, H.-K.; Vieira Da Cruz, A.; Compagne, N.; Jiménez-Castellanos, J.-C.; Müller, R.T.; Pradel, E.; Foong, W.E.; Malloci, G.; Ballée, A.; et al. Pyridylpiperazine-Based Allosteric Inhibitors of RND-Type Multidrug Efflux Pumps. *Nat. Commun.* **2022**, *13*, 115. [CrossRef]

84. Teelucksingh, T.; Thompson, L.K.; Zhu, S.; Kuehfuss, N.M.; Goetz, J.A.; Gilbert, S.E.; MacNair, C.R.; Geddes-McAlister, J.; Brown, E.D.; Cox, G. A Genetic Platform to Investigate the Functions of Bacterial Drug Efflux Pumps. *Nat. Chem. Biol.* **2022**, *18*, 1399–1409. [CrossRef] [PubMed]

85. Brandstätter, L.; Sokolova, L.; Eicher, T.; Seeger, M.A.; Briand, C.; Cha, H.; Cernescu, M.; Bohnert, J.; Kern, W.V.; Brutschy, B.; et al. Analysis of AcrB and AcrB/DARPin Ligand Complexes by LILBID MS. *Biochim. Et Biophys. Acta (BBA)—Biomembr.* **2011**, *1808*, 2189–2196. [CrossRef]

86. Yu, L.; Lu, W.; Wei, Y. AcrB Trimer Stability and Efflux Activity, Insight from Mutagenesis Studies. *PLoS ONE* **2011**, *6*, e28390. [CrossRef] [PubMed]

87. Seeger, M.A.; Schiefner, A.; Eicher, T.; Verrey, F.; Diederichs, K.; Pos, K.M. Structural Asymmetry of AcrB Trimer Suggests a Peristaltic Pump Mechanism. *Science* **2006**, *313*, 1295–1298. [CrossRef] [PubMed]

88. Murakami, S.; Nakashima, R.; Yamashita, E.; Matsumoto, T.; Yamaguchi, A. Crystal Structures of a Multidrug Transporter Reveal a Functionally Rotating Mechanism. *Nature* **2006**, *443*, 173–179. [CrossRef]

89. Sennhauser, G.; Amstutz, P.; Briand, C.; Storchenegger, O.; Grütter, M.G. Drug Export Pathway of Multidrug Exporter AcrB Revealed by DARPin Inhibitors. *PLoS Biol.* **2006**, *5*, e7. [CrossRef] [PubMed]

90. Seeger, M.A.; von Ballmoos, C.; Eicher, T.; Brandstätter, L.; Verrey, F.; Diederichs, K.; Pos, K.M. Engineered Disulfide Bonds Support the Functional Rotation Mechanism of Multidrug Efflux Pump AcrB. *Nat. Struct. Mol. Biol.* **2008**, *15*, 199–205. [CrossRef]

91. Nakashima, R.; Sakurai, K.; Yamasaki, S.; Nishino, K.; Yamaguchi, A. Structures of the Multidrug Exporter AcrB Reveal a Proximal Multisite Drug-Binding Pocket. *Nature* **2011**, *480*, 565–569. [CrossRef]

92. Eicher, T.; Cha, H.; Seeger, M.A.; Brandstätter, L.; El-Delik, J.; Bohnert, J.A.; Kern, W.V.; Verrey, F.; Grütter, M.G.; Diederichs, K.; et al. Transport of Drugs by the Multidrug Transporter AcrB Involves an Access and a Deep Binding Pocket That Are Separated by a Switch-Loop. *Proc. Natl. Acad. Sci. USA* **2012**, *109*, 5687–5692. [CrossRef]

93. Tam, H.-K.; Foong, W.E.; Oswald, C.; Herrmann, A.; Zeng, H.; Pos, K.M. Allosteric Drug Transport Mechanism of Multidrug Transporter AcrB. *Nat. Commun.* **2021**, *12*, 3889. [CrossRef]

94. Zwama, M.; Yamasaki, S.; Nakashima, R.; Sakurai, K.; Nishino, K.; Yamaguchi, A. Multiple Entry Pathways within the Efflux Transporter AcrB Contribute to Multidrug Recognition. *Nat. Commun.* **2018**, *9*, 124. [CrossRef]

95. Tam, H.-K.; Malviya, V.N.; Foong, W.-E.; Herrmann, A.; Malloci, G.; Ruggerone, P.; Vargiu, A.V.; Pos, K.M. Binding and Transport of Carboxylated Drugs by the Multidrug Transporter AcrB. *J. Mol. Biol.* **2020**, *432*, 861–877. [CrossRef] [PubMed]

96. Eicher, T.; Seeger, M.A.; Anselmi, C.; Zhou, W.; Brandstätter, L.; Verrey, F.; Diederichs, K.; Faraldo-Gómez, J.D.; Pos, K.M. Coupling of Remote Alternating-Access Transport Mechanisms for Protons and Substrates in the Multidrug Efflux Pump AcrB. *Elife* **2014**, *3*, e03145. [CrossRef]

97. Yue, Z.; Chen, W.; Zgurskaya, H.I.; Shen, J. Constant PH Molecular Dynamics Reveals How Proton Release Drives the Conformational Transition of a Transmembrane Efflux Pump. *J. Chem. Theory Comput.* **2017**, *13*, 6405–6414. [CrossRef]

98. Fischer, N.; Kandt, C. Porter Domain Opening and Closing Motions in the Multi-Drug Efflux Transporter AcrB. *Biochim. Et Biophys. Acta (BBA)—Biomembr.* **2013**, *1828*, 632–641. [CrossRef]

99. Murakami, S.; Nakashima, R.; Yamashita, E.; Yamaguchi, A. Crystal Structure of Bacterial Multidrug Efflux Transporter AcrB. *Nature* **2002**, *419*, 587–593. [CrossRef]

100. Cha, H.; Müller, R.T.; Pos, K.M. Switch-Loop Flexibility Affects Transport of Large Drugs by the Promiscuous AcrB Multidrug Efflux Transporter. *Antimicrob. Agents Chemother.* **2014**, *58*, 4767–4772. [CrossRef] [PubMed]

101. Kobayashi, N.; Tamura, N.; van Veen, H.W.; Yamaguchi, A.; Murakami, S. β-Lactam Selectivity of Multidrug Transporters AcrB and AcrD Resides in the Proximal Binding Pocket. *J. Biol. Chem.* **2014**, *289*, 10680–10690. [CrossRef] [PubMed]

102. Elkins, C.A.; Nikaido, H. Substrate Specificity of the RND-Type Multidrug Efflux Pumps AcrB and AcrD of *Escherichia coli* Is Determined Predominately by Two Large Periplasmic Loops. *J. Bacteriol.* **2002**, *184*, 6490–6498. [CrossRef] [PubMed]

103. Nikaido, H. Multidrug Efflux Pumps of Gram-Negative Bacteria. *J. Bacteriol.* **1996**, *178*, 5853–5859. [CrossRef]

104. Pos, K.M. Drug Transport Mechanism of the AcrB Efflux Pump. *Biochim. Biophys. Acta* **2009**, *1794*, 782–793. [CrossRef]

105. Zwama, M.; Nishino, K. Ever-Adapting RND Efflux Pumps in Gram-Negative Multidrug-Resistant Pathogens: A Race against Time. *Antibiotics* **2021**, *10*, 774. [CrossRef] [PubMed]

106. Ornik-Cha, A.; Wilhelm, J.; Kobylka, J.; Sjuts, H.; Vargiu, A.V.; Malloci, G.; Reitz, J.; Seybert, A.; Frangakis, A.S.; Pos, K.M. Structural and Functional Analysis of the Promiscuous AcrB and AdeB Efflux Pumps Suggests Different Drug Binding Mechanisms. *Nat. Commun.* **2021**, *12*, 6919. [CrossRef] [PubMed]

107. Schuster, S.; Vavra, M.; Kern, W.V. Evidence of a Substrate-Discriminating Entrance Channel in the Lower Porter Domain of the Multidrug Resistance Efflux Pump AcrB. *Antimicrob. Agents Chemother.* **2016**, *60*, 4315–4323. [CrossRef]

108. Ababou, A.; Koronakis, V. Structures of Gate Loop Variants of the AcrB Drug Efflux Pump Bound by Erythromycin Substrate. *PLoS ONE* **2016**, *11*, e0159154. [CrossRef]

109. Oswald, C.; Tam, H.-K.; Pos, K.M. Transport of Lipophilic Carboxylates Is Mediated by Transmembrane Helix 2 in Multidrug Transporter AcrB. *Nat. Commun.* **2016**, *7*, 13819. [CrossRef]

110. Reading, E.; Ahdash, Z.; Fais, C.; Ricci, V.; Wang-Kan, X.; Grimsey, E.; Stone, J.; Malloci, G.; Lau, A.M.; Findlay, H.; et al. Perturbed Structural Dynamics Underlie Inhibition and Altered Efflux of the Multidrug Resistance Pump AcrB. *Nat. Commun.* **2020**, *11*, 5565. [CrossRef]

111. Takatsuka, Y.; Chen, C.; Nikaido, H. Mechanism of Recognition of Compounds of Diverse Structures by the Multidrug Efflux Pump AcrB of *Escherichia Coli*. *Proc. Natl. Acad. Sci. USA* **2010**, *107*, 6559–6565. [CrossRef] [PubMed]

112. Vargiu, A.V.; Nikaido, H. Multidrug Binding Properties of the AcrB Efflux Pump Characterized by Molecular Dynamics Simulations. *Proc. Natl. Acad. Sci. USA* **2012**, *109*, 20637–20642. [CrossRef]

113. Aparna, V.; Dineshkumar, K.; Mohanalakshmi, N.; Velmurugan, D.; Hopper, W. Identification of Natural Compound Inhibitors for Multidrug Efflux Pumps of Escherichia Coli and Pseudomonas Aeruginosa Using In Silico High-Throughput Virtual Screening and *In Vitro* Validation. *PLoS ONE* **2014**, *9*, e101840. [CrossRef]

114. Kinana, A.D.; Vargiu, A.V.; May, T.; Nikaido, H. Aminoacyl β-Naphthylamides as Substrates and Modulators of AcrB Multidrug Efflux Pump. *Proc. Natl. Acad. Sci. USA* **2016**, *113*, 1405–1410. [CrossRef]

115. Zuo, Z.; Weng, J.; Wang, W. Insights into the Inhibitory Mechanism of D13-9001 to the Multidrug Transporter AcrB through Molecular Dynamics Simulations. *J. Phys. Chem. B* **2016**, *120*, 2145–2154. [CrossRef]

116. Dey, D.; Kavanaugh, L.G.; Conn, G.L. Antibiotic Substrate Selectivity of Pseudomonas Aeruginosa MexY and MexB Efflux Systems Is Determined by a Goldilocks Affinity. *Antimicrob. Agents Chemother.* **2020**, *64*, e00496-e20. [CrossRef]

117. Bohnert, J.A.; Schuster, S.; Seeger, M.A.; Fähnrich, E.; Pos, K.M.; Kern, W.V. Site-Directed Mutagenesis Reveals Putative Substrate Binding Residues in the *Escherichia Coli* RND Efflux Pump AcrB. *J. Bacteriol.* **2008**, *190*, 8225–8229. [CrossRef] [PubMed]

118. Morita, Y.; Nakashima, K.; Nishino, K.; Kotani, K.; Tomida, J.; Inoue, M.; Kawamura, Y. Berberine Is a Novel Type Efflux Inhibitor Which Attenuates the MexXY-Mediated Aminoglycoside Resistance in Pseudomonas Aeruginosa. *Front. Microbiol.* **2016**, *7*, 1223. [CrossRef] [PubMed]

119. Guan, L.; Nakae, T. Identification of Essential Charged Residues in Transmembrane Segments of the Multidrug Transporter MexB of *Pseudomonas Aeruginosa*. *J. Bacteriol.* **2001**, *183*, 1734–1739. [CrossRef]

120. Seeger, M.A.; von Ballmoos, C.; Verrey, F.; Pos, K.M. Crucial Role of Asp408 in the Proton Translocation Pathway of Multidrug Transporter AcrB: Evidence from Site-Directed Mutagenesis and Carbodiimide Labeling. *Biochemistry* **2009**, *48*, 5801–5812. [CrossRef] [PubMed]

121. Takatsuka, Y.; Nikaido, H. Threonine-978 in the Transmembrane Segment of the Multidrug Efflux Pump AcrB of *Escherichia Coli* Is Crucial for Drug Transport as a Probable Component of the Proton Relay Network. *J. Bacteriol.* **2006**, *188*, 7284–7289. [CrossRef]

122. Zhang, B.; Li, J.; Yang, X.; Wu, L.; Zhang, J.; Yang, Y.; Zhao, Y.; Zhang, L.; Yang, X.; Yang, X.; et al. Crystal Structures of Membrane Transporter MmpL3, an Anti-TB Drug Target. *Cell* **2019**, *176*, 636–648. [CrossRef]

123. Yang, X.; Hu, T.; Yang, X.; Xu, W.; Yang, H.; Guddat, L.W.; Zhang, B.; Rao, Z. Structural Basis for the Inhibition of Mycobacterial MmpL3 by NITD-349 and SPIRO. *J. Mol. Biol.* **2020**, *432*, 4426–4434. [CrossRef]

124. Schuster, S.; Kohler, S.; Buck, A.; Dambacher, C.; König, A.; Bohnert, J.A.; Kern, W.V. Random Mutagenesis of the Multidrug Transporter AcrB from Escherichia Coli for Identification of Putative Target Residues of Efflux Pump Inhibitors. *Antimicrob. Agents Chemother.* **2014**, *58*, 6870–6878. [CrossRef] [PubMed]

125. Belardinelli, J.M.; Yazidi, A.; Yang, L.; Fabre, L.; Li, W.; Jacques, B.; Angala, S.k.; Rouiller, I.; Zgurskaya, H.I.; Sygusch, J.; et al. Structure–Function Profile of MmpL3, the Essential Mycolic Acid Transporter from *Mycobacterium Tuberculosis*. *ACS Infect. Dis.* **2016**, *2*, 702–713. [CrossRef] [PubMed]